Journal of Colloid and Interface Science 345 (2010) 72–87

Contents lists available at ScienceDirect

Journal of Colloid and Interface Science

www.elsevier.com/locate/jcis

Electrokinetic phenomena in wavy channels

Alexander E. Malevich [a], Vladimir V. Mityushev [b], Pierre M. Adler [c,*]

[a] Dept. Mechanics and Mathematics, BSU, pr. Nezavisimosti 4, 220030 Minsk, Belarus
[b] Dept. Mathematics, Pedagogical University, ul. Podchorazych 2, Krakow 30-084, Poland
[c] UPMC-Sisyphe, tour 56, place Jussieu, 75252 Paris Cedex 05, France

ARTICLE INFO

Article history:
Received 10 November 2009
Accepted 14 January 2010
Available online 25 January 2010

Keywords:
Electroosmotic
Zeta potential
Rough channels
Formal expansion

ABSTRACT

Electroosmotic flows are studied in wavy channels by expanding the solution into a double series in terms of the dimensionless amplitudes and of the dimensionless zeta potential for a binary dilute electrolyte. The expansion technique by means of formal calculations is described. Some examples are illustrated and discussed for two and three dimensional channels. The importance of the varicose or sinuous character of the channels as well as the role of high frequency roughness are demonstrated. These features may be used for practical purposes in order to amplify or diminish coupling effects in an algebraic way.

1. Introduction

The study of electroosmotic flows through porous or dispersed media is important from a fundamental standpoint and for industrial applications. Among these applications, micro- and nanoflows are becoming more and more important [1]. The electroosmotic effects can be induced by two factors, namely when an electrolyte is submitted to an external electric field $\mathbf{E}$ and when a macroscopic pressure gradient $\overline{\nabla p}$ is applied to the flow. The electroosmotic phenomena are governed by a system of non-linear partial differential equations consisting of the Stokes equations, the convection–diffusion equations and the Poisson equation. All these three equations are coupled and this feature makes their resolution a very difficult computational problem.

The external "forcing factors" (or generalized forces) $\mathbf{E}$ and $\overline{\nabla p}$ generate a macroscopic current density $\mathbf{I}$ and a Darcy seepage velocity $\mathbf{u}$ which for small $\mathbf{E}$ and $\overline{\nabla p}$ are given by the linear formulae [2,3]

$$\begin{aligned} \mathbf{I} &= \boldsymbol{\sigma}\cdot\mathbf{E} - \boldsymbol{\alpha}\cdot\overline{\nabla p}, \\ \mathbf{u} &= \boldsymbol{\alpha}^{\mathrm{T}}\cdot\mathbf{E} - \tfrac{\mathbf{K}}{\mu}\cdot\overline{\nabla p}, \end{aligned} \tag{1}$$

where $\boldsymbol{\sigma}$ and $\mathbf{K}$ are the electric conductivity and permeability tensors; $\boldsymbol{\alpha}$ is the coupling electroosmotic tensor; the superscript T denotes the transposition operator. These three tensors are spherical for isotropic media. All the quantities in (1) are macroscopic quantities.

Since many experiments use rectangular channels, it was found interesting to evaluate these tensors for channels with wavy walls. Extended reviews of these processes before 1996 were given in [2,3]. Some recent contributions based on homogenization should be mentioned such as [4–7]. Several papers about analytical and numerical simulations in channels can be added. Electroosmotic flow and chaotic stirring were investigated by Qian and Bau [9] in rectangular cavities with a non-uniform zeta potential distribution ζ on the walls. The streaming current fields in an undulated channel were analytically studied by Brunet and Ajdari [10] thanks to a simplification of the electroosmotic equations. A numerical scheme was developed by Patankar and Hu [11] to simulate the electroosmotic flow between two channels. The lattice Boltzmann method was applied by Zu and Yan [12] to the electroosmotic flow between two parallel plates induced by moving vortices near the walls. Analytical solutions were derived by Gao et al. [13] for the flow of two liquids that relate the velocity profiles and flow rates to the liquid holdup, the aspect ratio of the microchannel, the viscosity ratio of the two liquids and the externally applied electric field. The basic concepts and a mathematical formulation of microflow control and pumping using electrokinetic effects were presented by Karniadakis et al. [1] with a discussion on numerical methods such as finite element and spectral element methods in stationary and moving domains. The physical mechanisms that lead to the charge inversion and flow reversal phenomena were discussed in [8].

Though the non-linear effects of the equations are taken into account in some of these references as well as some couplings such as between electrokinetic effect and elasticity [6], it was assumed that the ionic potentials (defined by Eq. (10)) satisfy separate

* Corresponding author. Fax: +33 1 44 27 45 88.
E-mail addresses: malevich@bsu.by (A.E. Malevich), vmityu@yahoo.com (V.V. Mityushev), pierre.adler@upmc.fr (P.M. Adler).

0021-9797/$ - see front matter © 2010 Elsevier Inc. All rights reserved.
doi:10.1016/j.jcis.2010.01.046

equations. This assumption decouples the electroosmotic equations since the ionic potential was calculated independently and substituted into the Stokes equation as an external force. The influence of the velocity on the ionic field was not taken into account. Therefore, the fully coupled equations were never addressed before to the best of our knowledge in an analytical way.

The linearization of the electroosmotic equations while preserving their coupling is a natural simplification after which the coupling tensor $\boldsymbol{\alpha}$ can be determined. Investigation of the dependence of $\boldsymbol{\alpha}$ on geometry is a challenging task. This dependence is known for simple geometries [2,3] (parallel plate channel, circular cylinder, semi-infinite space). For a plane channel of width $2b$, the tensors $\boldsymbol{\alpha}$ and $\mathbf{K}$ are simplified into the scalar coefficients α and K which are related by

$$\frac{\alpha}{\zeta K} = \frac{3}{\kappa^2 b^2}\left(\frac{\tanh(\kappa b)}{\kappa b} - 1\right). \tag{2}$$

The value κ^{-1} is known as the Debye–Hückel length [2,3].

In the present paper, the linear method [2,3] is used and the problem is solved for a curvilinear channel. An analytical method presented in [15] is applied to a channel enclosed by two wavy walls whose amplitude is proportional to the mean clearance of the channel multiplied by a small parameter ε. The dimensionless zeta potential ζ is taken as the second small parameter of the problem. The application of the analytical–numerical algorithm yields analytical formulae for the electric potential ψ, the ionic potentials Φ_i $(i = 1, 2)$ of a two-component dilute electrolyte, the fluid velocity $\mathbf{u}$ and the pressure p. These formulae include the spatial coordinates and ε in symbolic form. These formulae are subsequently applied to the determination of α.

This paper is organized as follows. Section 2 presents the basic equations. A 3D curvilinear channel is described in Section 2.1 in terms of the double Fourier series which describe its walls. Linearized equations are written in Section 2.2. In Section 2.3, dimensionless variables are introduced and equations are rewritten in these variables.

The electric potential ψ satisfies a separate boundary value problem which is solved in Section 3 by an expansion in terms of ε.

The main algorithm to determine the ionic potentials Φ_i $(i = 1, 2)$, the fluid velocity $\mathbf{u}$ and the pressure p is detailed in Section 4 where the second small parameter ζ is introduced. The main idea of the method is to apply perturbations in ε following [15]. Then, a cascade of partial differential equations for a plane channel with prescribed boundary data is derived. The successive problems are solved by expanding the unknown functions into double Fourier series of the spatial variables.

In Section 5, the coupling coefficient α is derived by using the Fourier series derived in the previous section. Then, examples computed up to $O(\varepsilon^3)$ and up to $O(\zeta^5)$ are presented and discussed.

In Section 6, a series of applications are made to two and three-dimensional channels. The role of the varicose or sinuous character of the channel is discussed as well as the importance of high frequency roughness.

Approximate analytical formulae for the velocity and for the coupling coefficient are given in Appendices A and B, respectively. The final formulae are presented in such a way that parameters can be changed and the corresponding plots obtained.

2. General

2.1. Geometry

Consider a 3D channel bounded by the walls

$$z = S^+(x,y) = b + b\varepsilon T(x,y), \qquad z = S^-(x,y) = -b + b\varepsilon B(x,y), \tag{3}$$

where (x,y,z) are the spatial coordinates; $T(x,y)$ and $B(x,y)$ are smooth periodic functions with the period $2L$ along x and y. $T(x,y)$ and $B(x,y)$ correspond to the top and bottom surfaces of the channel, respectively. ε is a dimensionless geometrical parameter which characterizes the roughness of the channel walls; it is generally assumed to be small with respect to 1. Fig. 1 illustrates these geometrical parameters for a two-dimensional channel.

The functions $T(x,y)$ and $B(x,y)$ can be expanded into double Fourier series which are conveniently presented in the complex form

$$T(x,y) = \sum_{s,t} T_{st} e^{\frac{i\pi}{L}(sx+ty)}, \qquad B(x,y) = \sum_{s,t} B_{st} e^{\frac{i\pi}{L}(sx+ty)}, \tag{4}$$

where i is the imaginary unity; s and t run over integer numbers from $-\infty$ to ∞. Since the functions $T(x,y)$ and $B(x,y)$ are real, their Fourier coefficients satisfy the relation

$$T_{-s,-t} = (T_{st})^*, \qquad B_{-s,-t} = (B_{st})^*, \tag{5}$$

where * stands for complex conjugation. Since the average positions of the top and bottom walls are equal to b and to $-b$, respectively, this implies

$$T_{00} = \int_{-L}^{L}\int_{-L}^{L} T(x,y)\,dx\,dy = 0, \qquad B_{00} = 0. \tag{6}$$

The functions $T(x,y)$ and $B(x,y)$ are assumed to be dimensionless and bounded by unity.

2.2. Equations

Consider a monovalent binary electrolyte close to equilibrium of density ρ, dynamic viscosity μ and electric permittivity ϵ_{el}. Let D_i denote the diffusion coefficient, $\Phi_i(x,y,z)$ the ionic potential of the ith component of the electrolyte $(i = 1, 2)$, $\mathbf{u}(x,y,z)$ the liquid velocity and $p(x,y,z)$ the pressure. Since stationary processes are addressed, the above quantities are functions of the spatial variables (x,y,z) only.

Let n_i^∞ denote the value of the ion concentration n_i $(i = 1,2)$ at zero potential, i.e., far from the solid walls. The ion concentration n_i is governed by the Boltzmann distribution

$$n_i = n_i^\infty \exp\left(-\frac{ez_i}{kT}\psi\right), \tag{7}$$

where $z_1 = -z_2 = 1$ is the ion's algebraic valency, k the Boltzmann constant, T the absolute temperature and ψ the electric potential of the solute. The electric charge density ρ can be expressed as [2–14]

$$\rho = e(n_1 - n_2) = -en^* \sinh\frac{e\psi}{kT}, \tag{8}$$

where $n^* = n_1^\infty + n_2^\infty$ and e is the arithmetic charge of the electron equal to 1.6×10^{-19} C.

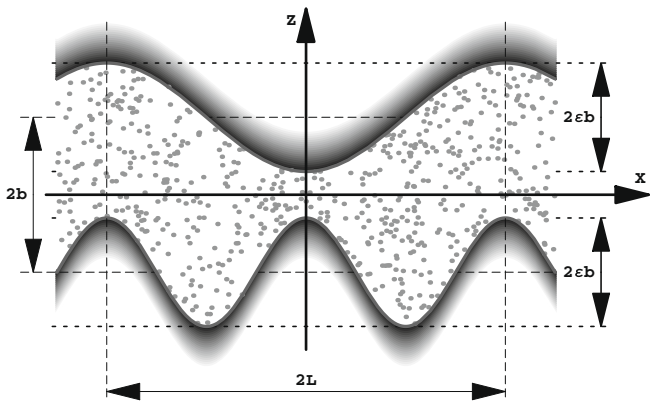

Fig. 1. Two-dimensional channel.

Introduce the Debye–Hückel length [2–14] κ^{-1}

$$\kappa = \sqrt{\frac{e^2 n^*}{\epsilon_{el} kT}}. \tag{9}$$

These phenomena are governed by the Poisson–Boltzmann equation, the convection diffusion equation and the Stokes equations which are coupled (see [2] for details). It is usual to assume that the external fields $\mathbf{E}$ and $\overline{\nabla p}$ are small which implies that the concentration distributions and other quantities do not differ significantly with respect to their equilibrium values denoted by the superscript ^{o}. The ionic potentials are introduced by means of relation (7)

$$n_i = n_i^\infty \exp\left(-\frac{ez_i}{kT}(\psi^o + \delta\psi + \Phi_i)\right) \tag{10a}$$

$$= n_i^o \exp\left(-\frac{ez_i}{kT}(\delta\psi + \Phi_i)\right), \tag{10b}$$

where $\delta\psi$ is a small local disturbance to the potential ψ. The Poisson–Boltzmann equation, the convection diffusion equation and the Stokes equations were linearized in [2,3]

$$\nabla^2\psi = \kappa^2\psi, \tag{11a}$$

$$\nabla^2\Phi_1 = \nabla\psi\cdot\left(\frac{e}{kT}\nabla\Phi_1 + \frac{1}{D_1}\mathbf{u}\right), \tag{11b}$$

$$\nabla^2\Phi_2 = \nabla\psi\cdot\left(-\frac{e}{kT}\nabla\Phi_2 + \frac{1}{D_2}\mathbf{u}\right), \tag{11c}$$

$$\mu\nabla^2\mathbf{u} = \nabla p + \frac{en^*}{2}\left[\left(-1+\frac{e}{kT}\psi\right)\nabla\Phi_1 + \left(1+\frac{e}{kT}\psi\right)\nabla\Phi_2\right], \tag{11d}$$

$$\nabla\cdot\mathbf{u} = 0, \quad S^-(x,y) < z < S^+(x,y), \tag{11e}$$

where ∇ stands for the gradient operator.

The boundary conditions were described in [2,3]

$$\psi\left[x,y,S^\pm(x,y)\right] = \zeta, \tag{12a}$$

$$\mathbf{u}\left[x,y,S^\pm(x,y)\right] = 0, \tag{12b}$$

$$p(L,y,z) - p(-L,y,z) = 2L\overline{\nabla p}, \tag{12c}$$

$$\frac{\partial\Phi_i}{\partial\mathbf{n}}\left[x,y,S^\pm(x,y)\right] = 0, \quad (i=1,2), \tag{12d}$$

where $\frac{\partial}{\partial\mathbf{n}}$ is the outward normal derivative to the surfaces (3). In accordance with (12a), the electric potential ψ is equal to the constant potential ζ on the walls; a constant charge density could have been implemented as well without changing the algorithm significantly. The velocity of the viscous fluid satisfies the no-slip condition (12b). Eq. (12c) corresponds to Poiseuille flow when the external pressure gradient $\overline{\nabla p}$ is applied along the x-axis. Here, the distinction between ∇p and $\overline{\nabla p}$ can be explained; the first gradient is a local pressure gradient at a given point (x,y,z) while $\overline{\nabla p}$ is the volume average of ∇p over the unit cell which corresponds to a spatial period. Eq. (12d) means that the walls are impermeable to the ions. Define the generalized pressure g by

$$g := p - \frac{en^*}{2}\Phi_1 + \frac{en^*}{2}\Phi_2, \tag{13}$$

g can be used to transform (11d) into

$$\mu\nabla^2\mathbf{u} = \nabla g + \frac{en^*}{2kT}\psi(\nabla\Phi_1 + \nabla\Phi_2). \tag{14}$$

The coupling tensor $\boldsymbol{\alpha}$ was introduced in [2,3] by linearizing the Poisson–Boltzmann equation (see formula [55a] from [2]). For a channel, it can be simplified into a scalar along the main direction of flow

$$\alpha = \frac{\epsilon_{el}\kappa^2}{\overline{\nabla p}}\langle\psi u\rangle, \tag{15}$$

where $\langle f(x,y,z)\rangle$ denotes the volume average of the function $f(x,y,z)$ over the unit cell.

Of course, the permeability K of the channel along the x-axis verifies Darcy law when $\mathbf{E}$ is zero

$$K = -\frac{\mu}{\overline{\nabla p}}\langle u\rangle, \tag{16}$$

where u is the x-component of the velocity $\mathbf{u}$.

2.3. Dimensionless variables and equations

In the present subsection, Eqs. (11)–(14) are written in a dimensionless form. $\varepsilon, T(x,y)$ and $B(x,y)$ are introduced above as dimensionless values. The position vector $\mathbf{r} = (x,y,z)$ is made dimensionless by κ^{-1}

$$\mathbf{r} = \kappa^{-1}\mathbf{r}'. \tag{17}$$

Other quantities are made dimensionless as follows

$$\zeta = \frac{kT}{e}\zeta', \quad \psi = \frac{kT}{e}\psi', \quad \Phi_i = \frac{kT}{e}\Phi_i', \quad n = \kappa^3 n',$$
$$\mathbf{u} = \frac{kTn^*}{\mu\kappa}\mathbf{u}', \quad D_i' = \frac{e^2\mu}{\epsilon_{el}k^2T^2}D_i, \quad g = kTn^*g', \tag{18}$$

(17) implies that the differential operator ∇ takes the following dimensionless form

$$\nabla' = \kappa^{-1}\nabla. \tag{19}$$

Following [2,3], introduce the dimensionless coefficient α' and the dimensionless permeability K'

$$\alpha = \frac{\epsilon_{el}kT}{e\mu}\alpha', \qquad K = \kappa^{-2}K'. \tag{20}$$

Introduction of these definitions into (15) and the use of (9) imply

$$\alpha' = A\langle\psi' u'\rangle \quad \text{with} \quad A = \frac{\epsilon_{el}\kappa^3}{\overline{\nabla p}}\left(\frac{kT}{e}\right)^2. \tag{21}$$

A similar transformation of (16) yields

$$K' = -A\langle u'\rangle. \tag{22}$$

Using (17), the problem (11)–(14) is rewritten in a dimensionless form. For shortness, primes are omitted below and in the rest of this paper

$$\nabla^2\psi = \psi, \tag{23a}$$

$$\nabla^2\Phi_1 = \nabla\psi\cdot\left(\nabla\Phi_1 + \frac{1}{D_1}\mathbf{u}\right), \tag{23b}$$

$$\nabla^2\Phi_2 = \nabla\psi\cdot\left(-\nabla\Phi_2 + \frac{1}{D_2}\mathbf{u}\right), \tag{23c}$$

$$\nabla^2\mathbf{u} = \nabla g + \frac{1}{2}\psi(\nabla\Phi_1 + \nabla\Phi_2), \tag{23d}$$

$$\nabla\cdot\mathbf{u} = 0. \tag{23e}$$

Eqs. (23) are fulfilled in the domain $S^-(x,y) < z < S^+(x,y)$. The boundary conditions become

$$\psi\left[x,y,S^\pm(x,y)\right] = \zeta, \tag{24a}$$

$$\mathbf{u}\left[x,y,S^\pm(x,y)\right] = 0, \tag{24b}$$

$$g(L,y,z) - g(-L,y,z) = \overline{\nabla g}, \tag{24c}$$

$$\frac{\partial\Phi_i}{\partial\mathbf{n}}\left[x,y,S^\pm(x,y)\right] = 0, \quad (i=1,2). \tag{24d}$$

The geometrical parameters of the channel can be arbitrary. All the other physical and chemical quantities are kept constant and equal to

$$\epsilon_{el} = 7.0 \times 10^{-10}\ \mathrm{F\,m^{-1}}, \quad e = 1.6 \times 10^{-19}\ \mathrm{C},$$
$$k = 1.38 \times 10^{-23}\ \mathrm{J\,K^{-1}}, \quad T = 300\ \mathrm{K}, \quad \mu = 1.0 \times 10^{-3}\ \mathrm{Pa\,s},$$
$$\zeta = -0.02\ \mathrm{V}, \quad 5 \times 10^{-9} \leqslant \kappa^{-1} \leqslant 25 \times 10^{-9}\ \mathrm{m}. \tag{25}$$

The range of κ^{-1} corresponds to the experimental one in [18]. If for illustration purposes, Na^+ and Cl^- are taken as cation and anion, the diffusivities are [18]

$$D_1 = 1.334 \times 10^{-9}\ \mathrm{m^2\,s^{-1}}, \quad D_2 = 2.032 \times 10^{-9}\ \mathrm{m^2\,s^{-1}}. \tag{26a}$$

The corresponding dimensionless values are

$$\zeta = -0.773, \quad D_1 = 2.846, \quad D_2 = 4.336. \tag{26b}$$

Of course, all these quantities may take other values depending on the nature of the ions and the physicochemical conditions. In the formal development, ζ is used in symbolic form. The linear character of Eqs. (23b), (23c), (23d), (23e), (24b), (24c) and (24d) imply that $\Phi_i, \mathbf{u}, \mathbf{g}$ are proportional to $\overline{\nabla g}$. Hence, without loss of generality $\overline{\nabla g}$ can be normalized.

The major features of this system can be summarized as follows. Eq. (23a) with the boundary condition (24a) can be considered as an independent boundary value problem. Eqs. (23b), (23c) and (24d) describe the ion distributions in the channels. Eqs. (23d), (23e), (24b) and (24c) are coupled and cannot be treated separately. This latter fact complicates the whole problem.

3. Electric potential

3.1. Derivation of the solution

Since ψ is not coupled with $\mathbf{u}$ and Φ_i ($i = 1,2$), it is solved independently in this section. It verifies

$$\nabla^2\psi = \psi, \quad \psi\left[x, y, S^{\pm}(x,y)\right] = \zeta. \tag{27}$$

ψ can be written as a series

$$\psi(x,y,z) = \zeta \sum_{k=0}^{\infty} \psi_k(x,y,z)\varepsilon^k. \tag{28}$$

The following Taylor formula for an analytic function F is applied to the boundary conditions (24a) [17]

$$F(Z + \Delta Z) = \sum_{n=0}^{\infty} \frac{\Delta Z^n}{n!} F^{(n)}(Z). \tag{29}$$

Let us apply (29) to ψ evaluated on the top surface, i.e., with $Z = b$ and $\Delta Z = b\varepsilon T(x,y)$

$$\psi[x,y,b + b\varepsilon T(x,y)] = \sum_{n=0}^{\infty} \frac{\varepsilon^n b^n T^n(x,y)}{n!} \frac{\partial^n \psi}{\partial z^n}(x,y,b). \tag{30}$$

Substituting (28) into (30) and rearranging the series yields

$$\psi[x,y,b + b\varepsilon T(x,y)] = \zeta \sum_{n=0}^{\infty} \varepsilon^n \sum_{k=0}^{n} \frac{b^k T^k(x,y)}{k!} \frac{\partial^k \psi_{n-k}}{\partial z^k}(x,y,b). \tag{31}$$

A similar formula can be derived on the bottom surface

$$\psi[x,y,-b + b\varepsilon B(x,y)] = -\zeta \sum_{n=0}^{\infty} \varepsilon^n \sum_{k=0}^{n} \frac{b^k B^k(x,y)}{k!} \frac{\partial^k \psi_{n-k}}{\partial z^k} \times (x,y,-b). \tag{32}$$

On the walls, ψ is equal to ζ. Use of (31) and (32) and selection of the coefficients with the same power of ε yields a classical cascade of problems for the plane channel $-b < z < b$. The zeroth problem is

$$\nabla^2\psi_0 = \psi_0, \quad \psi_0(x,y,b) = \psi_0(x,y,-b) = 1. \tag{33}$$

Therefore, ψ_0 depends only on z. Then, (33) becomes the boundary value problem for an ordinary differential equation

$$\frac{\mathrm{d}^2\psi_0}{\mathrm{d}z^2} = \psi_0, \quad -b < z < b, \quad \psi_0|_{z=b} = \psi_0|_{z=-b} = 1 \tag{34}$$

whose classical solution is

$$\psi_0(x,y,z) = \frac{\cosh z}{\cosh b}. \tag{35}$$

The next terms ψ_k can be constructed by recursive formulae. If the functions $\psi_1, \ldots, \psi_{n-1}$ are known, the nth problem of the cascade has the form

$$\nabla^2\psi_n = \psi_n, \tag{36a}$$

$$\psi_n(x,y,b) = -\sum_{k=1}^{n} \frac{b^k T^k(x,y)}{k!} \frac{\partial^k \psi_{n-k}}{\partial z^k}(x,y,b), \tag{36b}$$

$$\psi_n(x,y,-b) = -\sum_{k=1}^{n} \frac{b^k B^k(x,y)}{k!} \frac{\partial^k \psi_{n-k}}{\partial z^k}(x,y,-b), \tag{36c}$$

where the right-hand parts of (36b) and (36c) are known from the previous steps of the cascade. The problem (36) can be solved by the Fourier method [16]. ψ_n is expanded as a Fourier double series

$$\psi_n(x,y,z) = \sum_{s,t} \Psi_{nst}(z) e^{\frac{i\pi}{L}(sx+ty)}. \tag{37}$$

Convention for summation on s and t are the same as it is described for double Fourier series (4). In order to calculate the coefficients $\Psi_{nst}(z)$, substitute (37) into (36) and select the coefficients of $e^{\frac{i\pi}{L}(sx+ty)}$. Standard manipulations yield

$$\Psi_{nst}''(z) = \overline{\omega}_{st}^2 \Psi_{nst}(z), \quad -b < z < b, \quad \Psi_{nst}(b) = C_{nst}, \ \Psi_{nst}(-b) = D_{nst}, \tag{38}$$

where

$$\omega_{st} = \frac{\pi}{L}\sqrt{s^2 + t^2}, \quad \overline{\omega}_{st} = \sqrt{1 + \omega_{st}^2} = \sqrt{1 + \frac{\pi^2}{L^2}(s^2 + t^2)}, \tag{39}$$

C_{nst} and D_{nst} are the Fourier coefficients of the functions in the right parts of (36b) and (36c). It is worth noting that C_{nst} and D_{nst} are calculated by the functions ψ_j ($j = 0, 1, \ldots, n-1$) found in the previous steps. The solution of the problem (38) has the form

$$\Psi_{nst}(z) = \frac{1}{2}(C_{nst} + D_{nst})\frac{\cosh \overline{\omega}_{st} z}{\cosh \overline{\omega}_{st} b} + \frac{1}{2}(C_{nst} - D_{nst})\frac{\sinh \overline{\omega}_{st} z}{\sinh \overline{\omega}_{st} b}. \tag{40}$$

The proposed algorithm can be applied to any power of ε. Similar algorithms were given in [15] up to $O(\varepsilon^{30})$. In the present paper, the precision is restricted to $O(\varepsilon^2)$.

Application of (40) yields solutions to the first- and second-order problems in ε

$$\Psi_{1st}(z) = -\frac{b \tanh b}{2}\left[(T_{st} - B_{st})\frac{\cosh \overline{\omega}_{st} z}{\cosh \overline{\omega}_{st} b} + (T_{st} + B_{st})\frac{\sinh \overline{\omega}_{st} z}{\sinh \overline{\omega}_{st} b}\right], \tag{41}$$

where T_{st} and B_{st} are the Fourier coefficients of the boundary surfaces (see (4)). The functions $\Psi_{2st}(z)$ have the form (40) with $n = 2$ and with

$$C_{2st} = b^2 \sum_{p,q} T_{s-p,t-q}\left[\overline{\omega}_{st} \tanh b \ \frac{B_{pq} + T_{pq}\cosh 2\overline{\omega}_{st} b}{\sinh 2\overline{\omega}_{st} b} - \frac{T_{pq}}{2}\right],$$
$$D_{2st} = b^2 \sum_{p,q} B_{s-p,t-q}\left[\overline{\omega}_{st} \tanh b \ \frac{T_{pq} + B_{pq}\cosh 2\overline{\omega}_{st} b}{\sinh 2\overline{\omega}_{st} b} - \frac{B_{pq}}{2}\right]. \tag{42}$$

Convention for summation on p and q are the same as it is described for double Fourier series (4).

Therefore, the electric potential ψ has the form (28) and (37) where $\Psi_{nst}(z)$ is given by the recursive formula (40). The first

two functions $\Psi_{1st}(z)$ and $\Psi_{2st}(z)$ are written in the form (42). It is worth noting that the above formulae hold for arbitrary $T(x,y)$ and $B(x,y)$ if they are twice differentiable. The convergence radius of the series (28) was estimated in [15] as well as extensions to large ε and to non-smooth channels.

The electric charge density can be derived from (8) when ψ is known.

3.2. The linear approximation of the Poisson–Boltzmann equation

In the previous developments, the non-linear equation (8) is approximated by (27) with the classical approximation $\sinh X \approx X$ valid for small X. When the next term is taken into account, ψ for a plane channel ($\varepsilon = 0$) is given by

$$\psi(x,y,z) = \frac{\cosh z}{\cosh b}\zeta + \psi_{(3)}(x,y,z)\zeta^3 \tag{43a}$$

with

$$\psi_{(3)}(x,y,z) = \frac{1}{192\cosh^3 b}\left[\cosh 3z + 12z\sinh z - \frac{\cosh 3b + 12b\sinh b}{\cosh b}\cosh z\right] \tag{44}$$

The relative errors $\max_z|\frac{\psi_{(3)}}{\psi}|$ and $\max_z\frac{|\nabla\psi_{(3)}|}{|\nabla\psi|}$ which are given in Fig. 2 are seen to remain smaller than 5% across the channel. The relative error of the gradient is also estimated since it is present in the equations for Φ_i (23b) and (23c).

The disturbance due to ε does not essentially change the result because the final formulae contain the term $\varepsilon^2\zeta^3$ which is small even for the undisturbed terms caused by $\frac{\cosh z}{\cosh b}$. Therefore, the linear approximation (27) of $\nabla^2\psi = \sinh\psi$ is numerically justified for data such as (25) and (26).

4. General algorithm for the coupled problem

In this paper, expansions are restricted to the orders $O(\varepsilon^2)$ and $O(\zeta^4)$. Following [15], expansions on ε and ζ are used to reduce the coupled equations (23b), (23c), (23d), (23e), (24b), (24c) and (24d) to boundary value problems for the plane channel $-b < z < b$. The latter problem can be solved by the method of separated variables via power series in ζ and ε, and double Fourier series in x and y

$$\Phi_i(x,y,z) = \sum_{n,k=0}^{\infty}\zeta^n\varepsilon^k\Phi_{ink}(x,y,z) = \sum_{n,k=0}^{\infty}\zeta^n\varepsilon^k\sum_{s,t}\Phi_{inkst}(z)e^{\frac{i\pi}{L}(sx+ty)}, \quad (i=1,2), \tag{44a}$$

$$\mathbf{u}(x,y,z) = \sum_{n,k=0}^{\infty}\zeta^n\varepsilon^k\mathbf{u}_{nk}(x,y,z) = \sum_{n,k=0}^{\infty}\zeta^n\varepsilon^k\sum_{s,t}\mathbf{u}_{nkst}(z)e^{\frac{i\pi}{L}(sx+ty)}, \tag{44b}$$

where formally n and k can run from 0 to infinity. However, in the forthcoming symbolic computations, the largest values for them are equal to 4 and to 2, respectively. Hence, the sum on n and k is finite while the sum on s and t is an infinite double Fourier series. Further, sums with different subscripts are used. For instance, $\mathbf{u}_n$ means that an expansion in ζ is used, $\mathbf{u}_{nk}$ a double expansion in ζ and ε, $\mathbf{u}_{nkst}$ a series in ζ,ε and x,y. The function $g(x,y,z)$ is also expanded as

$$g(x,y,z) = \sum_{n,k=0}^{\infty}\zeta^n\varepsilon^k g_{nk}(x,y,z) = \sum_{n,k=0}^{\infty}\zeta^n\varepsilon^k\sum_{s,t}g_{nkst}(z)e^{\frac{i\pi}{L}(sx+ty)}. \tag{45}$$

Convention for summation on s and t are the same as it is described for double Fourier series (4).

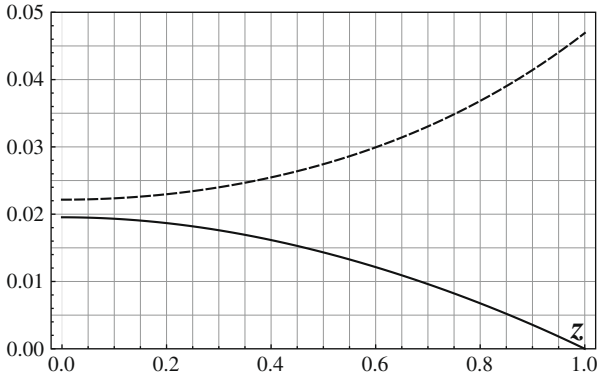

Fig. 2. The relative errors on ψ (solid line) and $\nabla\psi$ (broken line) as functions of z across the plane channel calculated by (43a) and (44). $b = 1$.

4.1. Ionic potentials

Eqs. (23b) and (23c) expanded in ζ yield the cascade

$$\nabla^2\Phi_{in} = \nabla\psi\cdot\left[(-1)^{i-1}\nabla\Phi_{i,n-1} + D_i^{-1}\mathbf{u}_{n-1}\right], \quad (i=1,2). \tag{46}$$

These equations directly show the coupling, i.e., the presence of lower order terms in ε in the right-hand side. A further expansion of (46) in ε yields

$$\sum_{k=0}^{\infty}\varepsilon^k\nabla^2\Phi_{1nk} = \sum_{k=0}^{\infty}\varepsilon^k\sum_{m=0}^{k}\nabla\psi_{k-m}\cdot\left(\nabla\Phi_{1,n-1,m} + D_1^{-1}\mathbf{u}_{n-1,m}\right), \tag{47}$$

where only one equation ($i = 1$) is written for shortness. When the coefficients in the same powers of ε are selected and when (35) is used which implies $\nabla\psi_0 = (0,0,\frac{\sinh z}{\cosh b})$, the following Poisson equations are derived

$$\nabla^2\Phi_{1nk} = F_{1nk}, \tag{48}$$

where

$$\begin{aligned} F_{10k} &= 0,\\ F_{1nk} &= \left(D_1^{-1}w_{n-1,k} + \tfrac{\partial\Phi_{1,n-1,k}}{\partial z}\right)\sinh z + \sum_{m=0}^{k-1}\nabla\psi_{k-m}\cdot(\nabla\Phi_{1,n-1,m}\\ &\quad + D_1^{-1}\mathbf{u}_{n-1,m}), \end{aligned} \tag{49}$$

where $\mathbf{u} = (u,v,w)$. The Fourier coefficients of F_{1nk} are calculated by

$$\begin{aligned} F_{1nkst}(z) &= \left(D_1^{-1}w_{n-1,kst} + \frac{\mathrm{d}\Phi_{1,n-1,kst}}{\mathrm{d}z}\right)\sinh z\\ &\quad + \frac{i\pi}{LD_1}\sum_{m=0}^{k-1}\sum_{p,q}\psi_{k-m,s-p,t-q}[(s-p)u_{n-1,mpq} + (t-q)v_{n-1,mpq}]\\ &\quad - \sum_{m=0}^{k-1}\sum_{p,q}\frac{\pi^2}{L^2}[(s-p)p + (t-q)q]\psi_{k-m,s-p,t-q}\Phi_{1,n-1,mpq}\\ &\quad + D_1^{-1}\sum_{m=0}^{k-1}\sum_{p,q}\frac{\mathrm{d}\psi_{k-m,s-p,t-q}}{\mathrm{d}z}. \end{aligned} \tag{50}$$

Convention for summation on p and q are the same as it is described for double Fourier series (4). An analogous formula holds for the second ionic potential

$$\begin{aligned} F_{2nkst}(z) &= \left(D_2^{-1}w_{n-1,kst} - \frac{\mathrm{d}\Phi_{2,n-1,kst}}{\mathrm{d}z}\right)\sinh z\\ &\quad + \frac{i\pi}{LD_2}\sum_{m=0}^{k-1}\sum_{p,q}\psi_{k-m,s-p,t-q}[(s-p)u_{n-1,mpq} + (t-q)v_{n-1,mpq}]\\ &\quad + \sum_{m=0}^{k-1}\sum_{p,q}\frac{\pi^2}{L^2}[(s-p)p + (t-q)q]\psi_{k-m,s-p,t-q}\Phi_{2,n-1,mpq}\\ &\quad + D_2^{-1}\sum_{m=0}^{k-1}\sum_{p,q}\frac{\mathrm{d}\psi_{k-m,s-p,t-q}}{\mathrm{d}z}. \end{aligned} \tag{51}$$

When Fourier series are used, (48) implies the ordinary differential equation

$$\frac{\mathrm{d}^2\Phi_{inkst}}{\mathrm{d}z^2}(z)-\omega_{st}^2\Phi_{inkst}(z)=F_{inkst}(z),\quad (i=1,2), \tag{52}$$

where ω_{st} has the form (39). The general solution of the differential equation (52) with non-zero ω_{st} is

$$\Phi_{inkst}(z)=C_{i1}\sinh\omega_{st}z+C_{i2}\cosh\omega_{st}z+\frac{1}{\omega_{st}}\int_{-b}^{z}\sinh[\omega_{st}(z-\xi)]F_{inkst}(\xi)\,\mathrm{d}\xi, \tag{53}$$

where C_{i1} and C_{i2} are undetermined constants which have to be found from the boundary conditions. The functions $F_{inkst}(z)$ are presented through the Fourier coefficients of the unknown functions found in the previous steps of the cascade by (50) and (51).

The boundary condition (24d) is transformed as follows. First, the unit vector $\mathbf{n}$ normal to the top surface is written in the form $\mathbf{n}=(0,0,1)-\varepsilon b\nabla T$ where $\nabla T=\left(\frac{\partial T}{\partial x},\frac{\partial T}{\partial y},0\right)$. An analogous formula can be derived for the bottom surface where $\mathbf{n}=(0,0,-1)+\varepsilon b\nabla B$. Then, (24d) expanded by ζ becomes

$$\sum_n\zeta^n\left[\frac{\partial\Phi_{in0}}{\partial z}+\sum_k\varepsilon^k\left(\frac{\partial\Phi_{ink}}{\partial z}-b\nabla\Phi_{in,k-1}\cdot\nabla T\right)\right]\Big|_{z=b}=0,\quad (i=1,2). \tag{54}$$

The selection of the coefficients with the same powers of ε in (54) yields a cascade of boundary conditions. It is convenient to expand the latter formulae in double Fourier series in terms of the functions found in the previous steps. These formulae for ε^k $(k=0,1,2)$ are

$$\begin{aligned}
&Z_{in0st}(T):=\tfrac{\mathrm{d}\Phi_{in0st}}{\mathrm{d}z}(b)=0,\\
&Z_{in1st}(T):=\tfrac{\mathrm{d}\Phi_{in1st}}{\mathrm{d}z}(b)=-b\sum_{p,q}T_{s-p,t-q}\left[F_{in0pq}(b)+\tfrac{\pi^2}{L^2}(sp+qt)\Phi_{in0pq}(b)\right],\\
&Z_{in2st}(T):=\tfrac{\mathrm{d}\Phi_{in2st}}{\mathrm{d}z}(b)=-b\sum_{p,q}T_{s-p,t-q}\left[F_{in1pq}(b)+\tfrac{\pi^2}{L^2}(sp+qt)\Phi_{in1pq}(b)\right]\\
&-\tfrac{b^2}{2}\sum_{p,q,p_1,q_1}T_{s-p-p_1,t-q-q_1}T_{p_1,q_1}\left[\tfrac{\mathrm{d}^3\Phi_{in0pq}}{\mathrm{d}z^3}(b)+\tfrac{2\pi^2}{L^2}(p_1p+q_1q)\tfrac{\mathrm{d}\Phi_{in0pq}}{\mathrm{d}z}(b)\right],
\end{aligned} \tag{55}$$

where F_{inkpq} $(i=1,2;\ k=0,1)$ is given by (50) and (51). (55) yield analogous formulae for the bottom surface when T is replaced by B, $F_{\dots}(b)$ by $F_{\dots}(-b)$ and $\Phi_{\dots}(b)$ by $\Phi_{\dots}(-b)$.

Substitution of (53) into (55) and solution of the corresponding linear algebraic system of second-order yields formulae for C_{i1} and C_{i2} in the kth step

$$\begin{aligned}
C_{i1}&=\frac{1}{2\sinh\omega_{st}b}\left(\frac{Z_{inkst}(T)-Z_{inkst}(B)}{\omega_{st}}+I_{inkst}\sinh\omega_{st}b-J_{inkst}\cosh\omega_{st}b\right),\\
C_{i}2&=\frac{1}{2\cosh\omega_{st}b}\left(\frac{Z_{inkst}(T)+Z_{inkst}(B)}{\omega_{st}}+I_{inkst}\sinh\omega_{st}b-J_{inkst}\cosh\omega_{st}b\right),
\end{aligned} \tag{56}$$

where $Z_{inkst}(T)$ and $Z_{inkst}(B)$ have the form (55),

$$\begin{aligned}
I_{inkst}&=\frac{1}{\omega_{st}}\int_{-b}^{b}F_{inkst}(\xi)\sinh(\xi)\,\mathrm{d}\xi,\\
J_{inkst}&=\frac{1}{\omega_{st}}\int_{-b}^{b}F_{inkst}(\xi)\cosh(\xi)\,\mathrm{d}\xi.
\end{aligned} \tag{57}$$

Formulae (53), (56) and (57) express the functions $\Phi_{inkst}(z)$ in closed form. Moreover, all integrals in these formulae can be calculated at each step with elementary functions, since each integral consists of hyperbolic trigonometric functions multiplied by polynomials. Integration of such a function yields a function of the same type which becomes an integrand at the next step of the cascade and so on.

4.2. Velocity

Computation of the velocity follows the lines presented in the previous section. However, the velocity satisfies the Stokes equations (23d) and (23e) which are more complicated than the Poisson equation.

Substituting the series (44b) into (23d) and (23e) and equating the coefficients with the same basic functions yield the following ordinary differential equations for the components of $\mathbf{u}_{nkst}=(u_{nkst},v_{nkst},w_{nkst})$

$$\begin{aligned}
&\tfrac{\mathrm{d}^2u_{nkst}}{\mathrm{d}z^2}(z)-\omega_{st}^2u_{nkst}(z)=\tfrac{i\pi s}{L}g_{nkst}(z)+\tfrac{i\pi}{L}F_{nkst}(z),\\
&\tfrac{\mathrm{d}^2v_{nkst}}{\mathrm{d}z^2}(z)-\omega_{st}^2v_{nkst}(z)=\tfrac{i\pi t}{L}g_{nkst}(z)+\tfrac{i\pi}{L}G_{nkst}(z),\\
&\tfrac{\mathrm{d}^2w_{nkst}}{\mathrm{d}z^2}(z)-\omega_{st}^2w_{nkst}(z)=\tfrac{\mathrm{d}g_{nkst}}{\mathrm{d}z}(z)+H_{nkst}(z),\\
&\tfrac{i\pi}{L}[su_{nkst}(z)+tv_{nkst}(z)]+\tfrac{\mathrm{d}w_{nkst}}{\mathrm{d}z}(z)=0,
\end{aligned} \tag{58}$$

where the functions F_{nkst}, G_{nkst} and H_{nkst} are expressed in terms of the functions $\Phi_{i,n-1,kpq}$ calculated in the previous steps

$$F_{0kst}=G_{0kst}=H_{0kst}=0, \tag{59}$$

$$\begin{aligned}
F_{nkst}&=\frac{1}{2}\sum_{m=0}^{k}\sum_{pq}p\psi_{k-m,s-p,t-q}(\Phi_{1,n-1,mpq}+\Phi_{2,n-1,mpq}),\\
G_{nkst}&=\frac{1}{2}\sum_{m=0}^{k}\sum_{pq}q\psi_{k-m,s-p,t-q}(\Phi_{1,n-1,mpq}+\Phi_{2,n-1,mpq}),\\
H_{nkst}&=\frac{1}{2}\sum_{m=0}^{k}\sum_{pq}\psi_{k-m,s-p,t-q}\left(\frac{\mathrm{d}\Phi_{1,n-1,mpq}}{\mathrm{d}z}+\frac{\mathrm{d}\Phi_{2,n-1,mpq}}{\mathrm{d}z}\right),\quad n>0.
\end{aligned} \tag{60}$$

As in (47) for the ionic potentials, the coupling is due to the lower order Φ-terms in the right-hand side.

Application of the Taylor formula (29) to the boundary conditions (24b) implies

$$\mathbf{u}_{n0st}(\pm b)=0,\ \mathbf{u}_{nkst}(b)=\mathbf{U}_{nkst},\qquad \mathbf{u}_{nkst}(-b)=\mathbf{V}_{nkst}, \tag{61}$$

where $\mathbf{U}_{nkst}$ and $\mathbf{V}_{nkst}$ are the Fourier coefficients of the functions

$$\begin{aligned}
&-\sum_{m=1}^{k}\frac{b^mT^m(x,y)}{m!}\frac{\partial^m\mathbf{u}_{n,k-m}}{\partial z^m}(x,y,b),\\
&-\sum_{m=1}^{k}\frac{b^mB^m(x,y)}{m!}\frac{\partial^m\mathbf{u}_{n,k-m}}{\partial z^m}(x,y,-b),
\end{aligned} \tag{62}$$

respectively. The first terms in ε $(k=1,2)$ can be written as

$$\begin{aligned}
\mathbf{U}_{n1st}&=-b\sum_{p,q}T_{s-p,t-q}\frac{\mathrm{d}\mathbf{u}_{n0pq}}{\mathrm{d}z}(b),\qquad \mathbf{V}_{n1st}=-b\sum_{p,q}B_{s-p,t-q}\frac{\mathrm{d}\mathbf{u}_{n0pq}}{\mathrm{d}z}(-b),\\
\mathbf{U}_{n2st}&=-b\sum_{p,q}T_{s-p,t-q}\frac{\mathrm{d}\mathbf{u}_{n1pq}}{\mathrm{d}z}(b)-\frac{b^2}{2}\sum_{p,q}\sum_{p_1,q_1}T_{s-p-p_1,t-q-q_1}\frac{\mathrm{d}^2\mathbf{u}_{n0pq}}{\mathrm{d}z^2}(b),\\
\mathbf{V}_{n2st}&=-b\sum_{p,q}B_{s-p,t-q}\frac{\mathrm{d}\mathbf{u}_{n1pq}}{\mathrm{d}z}(-b)-\frac{b^2}{2}\sum_{p,q}\sum_{p_1,q_1}B_{s-p-p_1,t-q-q_1}\frac{\mathrm{d}^2\mathbf{u}_{n0pq}}{\mathrm{d}z^2}(-b).
\end{aligned} \tag{63}$$

Then, the general system of ordinary differential equations (58) is solved with the boundary conditions (63). The cases $\omega_{st}=0$ and $\omega_{st}\neq0$ must be investigated separately.

The detailed solution is given in Appendix A.

5. The coupling coefficient

5.1. General

The dimensionless coupling coefficient is related to the dimensionless electric potential and the dimensionless velocity by formula (15) where primes are omitted in non-dimensional values for shortness. The averaged $\langle\psi u\rangle$ can be calculated by the double integral

$$\langle \psi u \rangle = \frac{1}{|\tau|} \int_{-L}^{L} \int_{-L}^{L} \mathrm{d}x\,\mathrm{d}y \int_{S^-(x,y)}^{S^+(x,y)} \psi u \,\mathrm{d}z, \tag{64}$$

where $|\tau|$ is the dimensionless volume of the periodicity cell

$$|\tau| = \int_{-L}^{L} \int_{L}^{L} (S^+(x,y) - S^-(x,y))\,\mathrm{d}x\,\mathrm{d}y = 8bL^2. \tag{65}$$

The integral (65) is calculated by application of (3)–(6).

The division of the dimensionless coupling coefficient (21) by the dimensionless permeability (22) and by the dimensionless parameter ζ yields

$$\frac{\alpha}{\zeta K} = -\frac{1}{\zeta} \frac{\langle \psi u \rangle}{\langle u \rangle}. \tag{66}$$

The zero approximation (A2) for u and the zero approximation $\Psi_0 = \zeta \psi_0$ derived from (35) and (A2) imply that

$$\langle u_{00} \rangle = -\frac{\overline{\nabla p}\, b^2}{3}, \quad \langle \Psi_0 u_{00} \rangle = \zeta \overline{\nabla p} \left(\frac{\tanh b}{b} - 1 \right). \tag{67}$$

Division of the left equation by the right one in (67) and substitution of the result into (66) yield the dimensionless version of (2)

$$\frac{\alpha_0}{\zeta K_0} = \frac{3}{b^2} \left(\frac{\tanh b}{b} - 1 \right), \tag{68}$$

where α_0 and K_0 denote the coupling coefficient and the permeability for the plane channel.

5.2. Expansion of the coupling coefficient

Calculation of $\langle \psi u \rangle$ and $\langle u \rangle$ for wavy channels requires their ε-expansion. These expressions are obtained in Appendix B. $\langle \psi u \rangle$ is given by (B7) and (B9) with an accuracy $O(\varepsilon^2)$ and $O(\zeta^4)$. $\langle u \rangle$ is given by (B10) and (B11).

6. Applications

6.1. Two examples

As a first application of the algorithms, consider the two-dimensional channel $\mathscr{V}_1$ bounded by the walls (see Table 1)

$$z = b + b\varepsilon \cos x, \qquad z = -b - b\varepsilon \cos x, \tag{69}$$

i.e., $L = \pi$, $T_{-1,0} = T_{1,0} = -B_{-1,0} = -B_{1,0} = 0.5$; the other Fourier coefficients T_{st} and B_{st} are equal to zero. In this example, the electric potential up to $O(\varepsilon^3)$ has the form

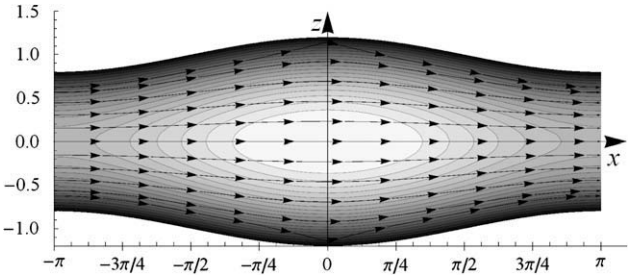

Fig. 3. The level plot of ψ and streamlines in the channel (69) with $b = 1$, $\zeta = -0.773$, $\varepsilon = 0.2$ and $L = \pi$.

$$\psi = \frac{\zeta}{\cosh b} \left\{ \cosh z - \varepsilon b \cos x \frac{\cosh \sqrt{2} z}{\cosh \sqrt{2} b} \sinh b - \frac{\varepsilon^2 b^2}{4} \left[\cos 2x \frac{\cosh \sqrt{5} z}{\cosh \sqrt{5} b} \times (\cosh b - 2\sqrt{2} \sinh b \tanh \sqrt{2} b) + \cosh z (1 - 2\sqrt{2} \tanh b \tanh \sqrt{2} b) \right] \right\}. \tag{70}$$

A level plot of ψ is displayed in Fig. 3.

Then, the permeability K, the coupling coefficient α and the combination $A = \frac{\alpha}{\zeta K}$ are obtained as

$$K = 0.053052 + \varepsilon^2 (-0.190647 - 0.000229\zeta^2 - 2.55 \times 10^{-6} \zeta^3 + 3.27 \times 10^{-7} \zeta^4)$$

$$\alpha = -0.037944\zeta + \varepsilon^2 (0.091295\zeta + 0.000160\zeta^3 + 1.79 \times 10^{-6} \zeta^4 - 2.29 \times 10^{-7} \zeta^5)$$

$$\frac{\alpha}{\zeta K} = -0.715218 + \varepsilon^2 (-0.849336 - 0.000061\zeta^2 - 6.86 \times 10^{-7} \zeta^3 + 8.70 \times 10^{-8} \zeta^4).$$

These formulae can be noted as

$$K = K_{00} + \varepsilon^2 (K_{02} + K_{22}\zeta^2 + K_{32}\zeta^3 + K_{42}\zeta^4), \tag{71a}$$

$$\alpha = \alpha_{10}\zeta + \varepsilon^2 (\alpha_{12}\zeta + \alpha_{32}\zeta^3 + \alpha_{42}\zeta^4 + \alpha_{52}\zeta^5), \tag{71b}$$

$$A = \frac{\alpha}{\zeta K} = A_{00} + \varepsilon^2 (A_{02} + A_{22}\zeta^2 + A_{32}\zeta^3 + A_{42}\zeta^4) \tag{71c}$$

where the first index n corresponds to the order in ζ, and the second one k to the order in ε (see Tables 2, C.1–C.3 and C.4).

A first remark which can be made on these coefficients is that K_{n2}, $\alpha_{n+1,2}$ and A_{n2} are very small when $n > 2$. Therefore, the correction due to higher orders in ζ because of the coupling between the ionic potentials and the flow is usually very small. It should be noticed that the discussion will be mostly focused on K_{02} and α_{12} in the following.

Table 1
The two-dimensional configurations addressed in Section 6.2. Some of them are illustrated in Fig. 4.

Channel	ω	Top wall		Bottom wall		Comment
		c_{top}	s_{top}	c_{bot}	s_{bot}	
$\mathscr{V}_n$	n	1	0	−1	0	$n = 1, \ldots, 12$
$\mathscr{S}_n$	n	1	0	1	0	$n = 1, \ldots, 12$
$\mathscr{I}_n$	$1, 2, n$	$\frac{8}{11}, 0, \frac{1}{10}$	$0, -\frac{4}{9}, 0$	$-\frac{8}{11}, 0, -\frac{1}{10}$	$0, \frac{4}{9}, 0$	$n = 3, \ldots, 12$
$\mathscr{C}_1$	$1, 3, 5, 7, 9$	$1, -\frac{1}{3}, \frac{1}{5}, -\frac{1}{7}, \frac{1}{9}$	0	$-1, \frac{1}{3}, -\frac{1}{5}, \frac{1}{7}, -\frac{1}{9}$	0	
$\mathscr{C}_2$	$5, 13$	$0, \frac{1}{2}$	$-\frac{1}{2}, 0$	$0, -\frac{1}{2}$	$\frac{1}{2}, 0$	
$\mathscr{C}_3$	$5, 8, 13$	$0, 0, \frac{1}{2}$	$-\frac{1}{2}, 0, 0$	$0, \frac{1}{2}, 0$	$0, 0, -\frac{1}{2}$	
$\mathscr{C}_4$	$1, 2$	$\frac{8}{11}, 0$	$0, -\frac{4}{9}$	$\frac{8}{11}, 0$	$0, -\frac{4}{9}$	
$\mathscr{C}_5$	$1, 2, 3, 4, 5, 6$	$\frac{1}{6}, \frac{1}{6}, \frac{1}{6}, \frac{1}{6}, \frac{1}{6}, \frac{1}{6}$	0	$-\frac{1}{6}, -\frac{1}{6}, -\frac{1}{6}, -\frac{1}{6}, -\frac{1}{6}, -\frac{1}{6}$	0	
$\mathscr{C}_6$	1	0	0	−1	0	

Table 2
The fitted linear dependence of coefficients K_{02}, α_{12} and A_{02} of wave number n (see Eqs. (71) and Table 1).

Channel	$K_{02}(n)$	$\alpha_{12}(n)$	$A_{02}(n)$
$\mathcal{V}_n$	$0.07725240 - 0.15891730n$	$-0.09578348 + 0.10634841n$	$-0.76399530 - 0.13782850n$
$\mathcal{S}_n$	$0.08188105 - 0.15939037n$	$-0.09918129 + 0.10669565n$	$-0.76564110 - 0.13766085n$
$\mathcal{I}_n$	$-0.15542495 - 0.00158340n$	$0.07637030 + 0.00105797n$	$-0.65582033 - 0.00140439n$
$\mathcal{V}_n^{3d}$	0.07957747	$-0.10247843 - 0.01431426n$	$-0.85884652 - 0.26981736n$
$\mathcal{S}_n^{3d}$	0.07957747	$-0.10252508 - 0.01430947n$	$-0.85972588 - 0.26972724n$

At this point, it should be recalled that the non-linear equation (8) has been linearized by $\sinh\psi \approx \psi$ and that the resulting potential has been hardly modified as it was discussed in Section 3.2.

A second example can be detailed in order to illustrate the three-dimensional calculations. Consider the channel $\mathcal{C}_1^{3d}$ bounded by the walls (see Table 3 and Fig. 8c)

$$z = 1 + \varepsilon\cos x\cos y, \qquad z = -1 - \varepsilon\cos x\cos y, \tag{72}$$

i.e., $b = 1$, $L = \pi$, $T_{\pm1,\pm1} = -B_{\pm1,\pm1} = 0.25$; the other Fourier coefficients T_{st} and B_{st} are equal to zero.

The electric potential up to $O(\varepsilon^3)$ has the form

$$\psi = 0.64800\zeta\Big\{\cosh z - 0.40322\varepsilon\cos x\cos y\cosh(\sqrt{3}z) + \varepsilon^2\Big[0.24102\cos 2y\cosh(\sqrt{5}z) + 0.10366\cos 2x\cos 2y\cosh 3z\Big]\Big\}. \tag{73}$$

The corresponding expansions (71) are given by

$$K = 0.053052 + \varepsilon^2(-0.035442 - 0.000034\zeta^2 - 3.28\times10^{-7}\zeta^3 + 4.10\times10^{-8}\zeta^4),$$
$$\alpha = -0.037944\zeta + \varepsilon^2(-0.003504\zeta + 0.000024\zeta^3 + 2.29\times10^{-7}\zeta^4 - 2.87\times10^{-8}\zeta^5),$$
$$\frac{\alpha}{\zeta K} = -0.715218 + \varepsilon^2(-0.543864 - 0.000010\zeta^2 - 1.00\times10^{-7}\zeta^3 + 1.22\times10^{-8}\zeta^4).$$

The same comments as before can be made on these coefficients (see Tables 2 and C.5).

Table 3
The three-dimensional configurations addressed in Section 6.3. Some of them are illustrated in Fig. 8.

Channel	Top wall	Bottom wall	Comment
$\mathcal{V}_n^{3d}$	$\cos ny$	$-\cos ny$	$n = 1,\ldots,12$
$\mathcal{S}_n^{3d}$	$\cos ny$	$\cos ny$	$n = 1,\ldots,12$
$\mathcal{C}_1^{3d}$	$\cos x\cos y$	$-\cos x\cos y$	
$\mathcal{C}_2^{3d}$	$\cos x\cos y$	$-\sin x\cos y$	

6.2. An overview of the analytical calculations in 2d

Calculations are better made in complex notations (4), but representation is easier with real components. The various channels are studied for integer values of the pulsation ω, i.e., the walls are obtained by superposing functions of the form $\cos\omega_1 x$ and $\sin\omega_2 x$ where ω_1 and ω_2 are integer. The following notation is used. The various pulsations are given by the vector ω and the corresponding amplitudes of the cos and sin are given by the vectors c

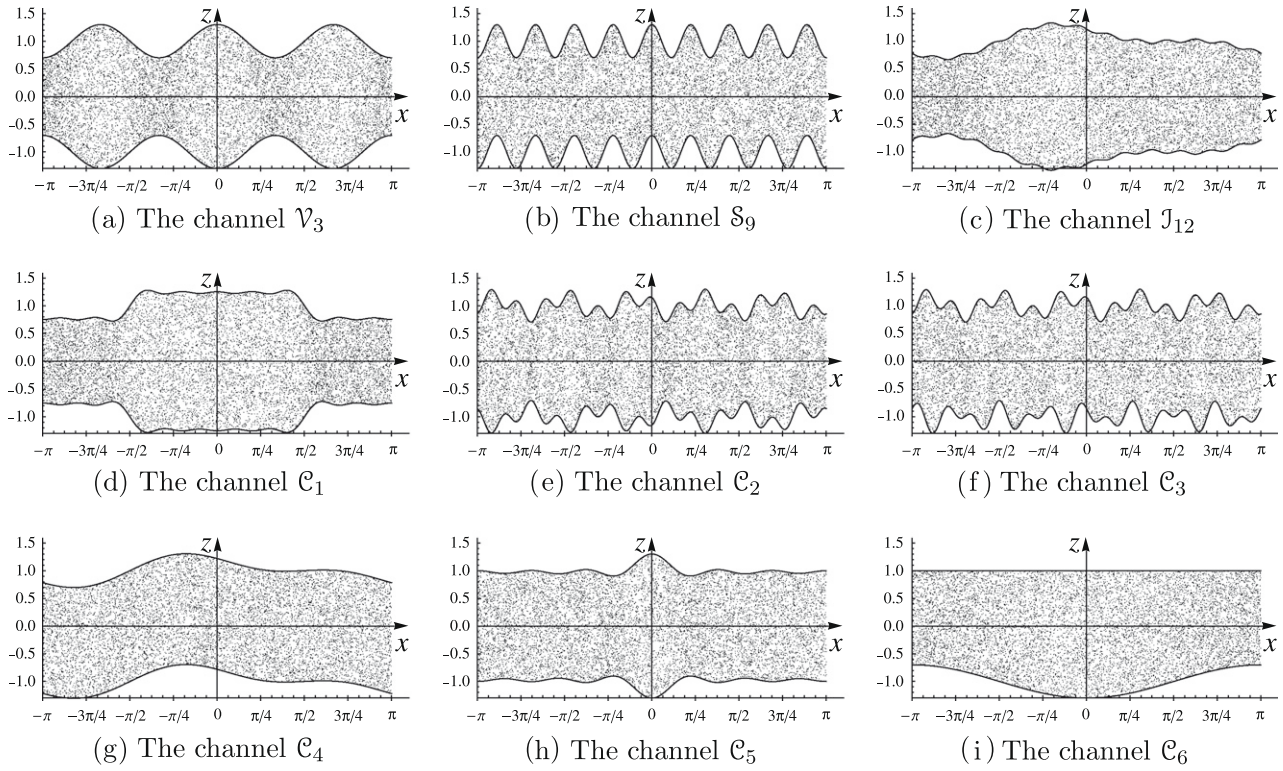

Fig. 4. Some examples of two-dimensional channels (Table 1).

and s. These notations can be illustrated by the following example; $\omega = (1,2,3),\ c = (2,\frac{1}{3},1),\ s = (0,2,0)$ denote the wall

$$S(x,y) = 2\cos x + \frac{1}{3}\cos 2x + 2\sin 2x + \cos 3x. \tag{74}$$

The cases studied in two dimensions are summarized in Table 1. Some of them are illustrated in Fig. 4. Note that the configurations $\mathscr{V}_n$ correspond to the channel limited by $-1-\varepsilon\cos nx \leqslant z \leqslant 1+\varepsilon\cos nx$. Of course, the importance of the corrections to the case of a straight channel depends on the value of ϵ and ζ. Whenever, the channel is very smooth and $|\zeta|$ small, the following corrections are negligible.

The results are given in Tables 2, C.1–C.4. They can by summarized as follows.

6.2.1. General properties

Let us first comment the results relative to the configurations $\mathscr{V}_1$, $\mathscr{S}_1$ and $\mathscr{I}_1$.

K_{02} is always negative and it is most of the times of order 1. The sign and the variations in the orders of magnitude are certainly related to the linear character of the streamlines. It is indeed a well known fact that viscous dissipation is minimal for straight streamlines.

α_{10} is always negative. The opposite is true for α_{12} which is almost always positive which means that the part of α depending on ε^2 (see formula (71b)) is an increasing function of $-\zeta$. This behavior is in agreement with physical intuition since wall oscillations which increase the solid surface are likely to increase electroosmotic effects. The only counterexample is for the purely sinuous channel $\mathscr{S}_1$; but, it should be noticed that in this case $|\alpha_{12}|$ is small when compared with the other configurations. The other coefficients α_{n2} ($n \geqslant 3$) may have different signs. In the sinuous mode, illustrated by the channels $\mathscr{I}_n$, some of them indeed change sign.

A last general comment can be made on all these coefficients. Usually, only the 2 first ones are of order 1. There are at least 2 or 3 orders of magnitude between α_{12} and α_{32} for instance which means that the higher order term is completely negligible. It is important also to notice that numerical computations based on discretization techniques could not reach such a precision easily while this is done without any difficulty with the analytical technique presented in this paper; usually, the numerical task consists in simple quadratures, i.e., in one-dimensional integrations of smooth functions; this does not present any problem and this can be done with an excellent precision.

The same is true for K_{02} and K_{22}; K_{22} is about two orders of magnitude smaller than K_{02}.

6.2.2. Influence of the wave number

Because of its importance in real channels, the influence of large wave numbers was studied for its own sake. First, this influence was addressed for the series of varicose channels denoted as $\mathscr{V}_n$. The coefficients K_{02} and α_{12} are plotted in Figs. 5 and 6 where they are seen to be increasing functions of n; obviously, the absolute value of the coupling increases with n to the expense of a larger viscous dissipation. It should be noticed that K_{02} and α_{12} are linear functions of the wave number n which are fitted for $4 \leqslant n \leqslant 12$; no obvious explanation was found for this very interesting behavior. The coefficients are given in Table 2.

These calculations on the influence of roughness with large wave numbers on K and α were extended in two ways because of their practical importance. First, channels in the sinuous mode were investigated. More precisely, let us denote by $\mathscr{S}_n$ the channels limited by $-1+\varepsilon\cos nx \leqslant z \leqslant 1+\varepsilon\cos nx$. The corresponding coefficients K_{02} and α_{12} are plotted in Fig. 5 and gathered in Table 2. K_{02} is always negative and its absolute value is an increasing value of n. It is remarkably close to the values obtained

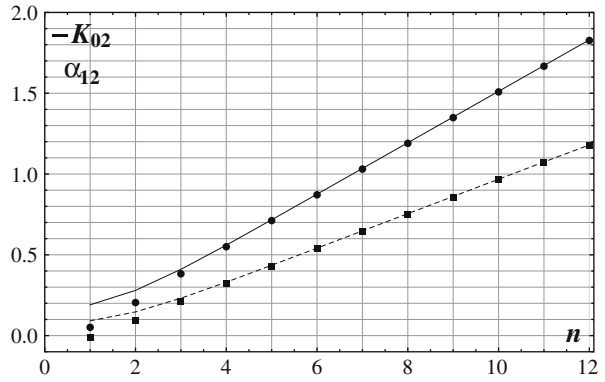

Fig. 5. Dependence of the coefficients $-K_{02}$ and α_{12} of pulsation n for the two-dimensional channels $\mathscr{V}_n$ and $\mathscr{S}_n$. Data are for: $\mathscr{V}_n$: $-K_{02}$ (solid line), α_{12} (broken line); $\mathscr{S}_n$: $-K_{02}$ (•), α_{12} (■).

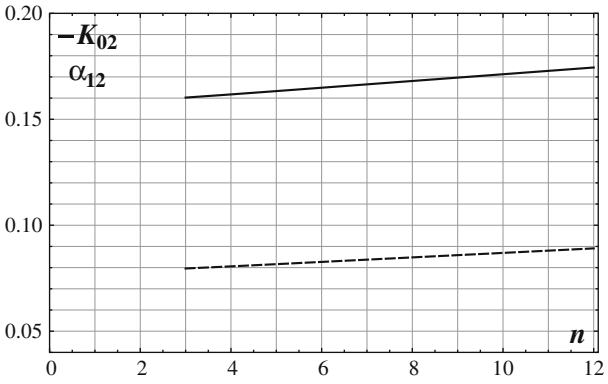

Fig. 6. The coefficients $-K_{02}$ (solid line) and α_{12} (broken line) as functions of the wave number n for the channels $\mathscr{I}_n$.

for the varicose channels $\mathscr{V}_n$ again without any obvious explanation. Moreover, the difference between the two values decreases with n; for instance $K_{02} = -0.280$ for $\mathscr{V}_2$, and -0.208 for $\mathscr{S}_2$, while the two values coincide and are equal to -1.83028 for $\mathscr{V}_{12}$ and $\mathscr{S}_{12}$. Of course, the higher order coefficients in the expansion of K are different.

With the remarkable exception of $n = 1$, α_{12} is always positive for $\mathscr{S}_n$ and it is also an increasing function of n. It becomes rapidly of order 1. The same phenomenon as for K_{02} occurs, namely the difference with α_{12} obtained for $\mathscr{V}_n$ decreases with n.

This increase of coupling with n is an effect which can be practically important since it means that a roughness with a small wave length has a larger influence than a roughness with the same amplitude, but a longer wave length.

This effect was further investigated on the channels $\mathscr{I}_n$ which result from the superpositions of three terms $\omega = (1,2,n)$, $c_{top} = -c_{bot} = (\frac{8}{11},0,\frac{1}{10})$, $s_{top} = -s_{bot} = (0,-\frac{4}{9},0)$. The wave number n of the last cosinus was successively increased from 3 to 12 while keeping constant the other characteristics. The same trends as in $\mathscr{V}_n$ are seen for K_{02} and α_{12} when n increases (see Fig. 6). The observed variations are less important because the amplitude of $\sin nx$ is equal to $\frac{1}{10}$ and therefore significantly smaller that the others. However, the important fact is that the trend is still present. Linear fits are also given in Table 2. It is seen that the fit is excellent for all values of n, i.e., $3 \leqslant n \leqslant 12$.

6.3. An overview of the analytical calculations in 3d

A similar set of calculations though significantly less extensive was made in 3d. The studied cases are summarized in Table 3 with notations analogous to Table 1.

It is interesting to see that K_{02} is always positive and α_{12} is always negative for the channels $\mathscr{V}_n^{3d}$ and $\mathscr{S}_n^{3d}$.

Let us now look at the influence of large wave numbers in a 3d channel. Two cases can be considered as illustrated in Fig. 8. The oscillations are so to speak parallel to the flow since the other case was already investigated in the previous section; the channels can be again either varicose or sinuous. The equations for the walls are

$$T = \cos ny, \qquad B = \pm \cos ny. \tag{75}$$

Results for K_{02} and α_{12} are given in Fig. 7 and in Table C.5. The first interesting feature is that K_{02} is now always positive and constant whatever the value of n and the channel type. This remark was not made before to the best of our knowledge; it is certainly related to the fact that streamlines are straight and that the Stokes equations are reduced to a two-dimensional Poisson equation.

The second specific feature is that α_{12} is always negative whatever the channel type (see Fig. 7). $|\alpha_{12}|$ is an increasing function of n as in two dimensions. $|\alpha_{12}|$ depends slightly on the channel type for small n, but this is influence disappears rapidly when n increases.

Again the coefficients K_{02} and α_{12} are well fitted by linear relations for $4 \leqslant n \leqslant 12$; the values of the coefficients are given in Table 2.

6.4. Discussion

It might be useful to summarize the analytical–numerical algorithm which was devised in order to calculate the coefficients α and A to $O(\varepsilon^3)$ and $O(\zeta^4)$. The expansion in ε is used to reduce the electroosmotic equations. (23)-(24) for a curvilinear channel to equations for a plane channel $-b \leqslant z \leqslant b$. The latter problem is reduced to a cascade of boundary value problems for ordinary differential equations by expansions in ζ and by using the method of separated variables. As a result ψ, Φ_i and $\mathbf{u}$ are written as double Fourier series in x, y with coefficients in z (see formulae (37), (40) and (42) for ψ; (53), (56) and (57) for Φ_i; (59), (60) and (63) for $\mathbf{u}$).

The coefficients α and A are determined by integrating over the unit cell. The considered triple integrals are first reduced to successive integrals in x, y and in z

$$\int_{-L}^{L}\int_{-L}^{L} \mathscr{F}(x,y)\,\mathrm{d}x\,\mathrm{d}y, \tag{76}$$

where $\mathscr{F}(x,y)$ has the form (B1). First, the integral $\mathscr{F}(x,y)$ is reduced to the form (B3) which contains an ordinary integral

$$\int_{-b}^{b} f(x,y,z)\,\mathrm{d}z, \tag{77}$$

The integral (77) is calculated by expanding $f(x,y,z)$ as a double Fourier series in x, y. Only the zero term ($s = t = 0$) yields a non-zero integral in (76). Therefore, in order to calculate the triple integral (76) over the curvilinear unit cell $S^-(x,y) \leqslant z \leqslant S^+(x,y)$, $-L \leqslant x,\ y \leqslant L$, we need to compute a single ordinary integral in z for the zero Fourier coefficient $f_{00}(z)$ of the function $f(x,y,z)$.

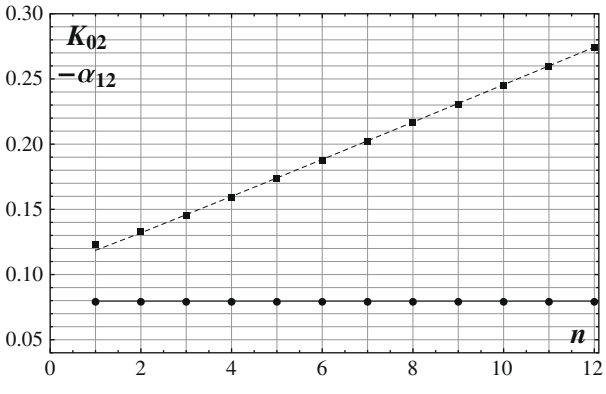

Fig. 7. The coefficients K_{02} and $-\alpha_{12}$ as functions of the wave number n for the three-dimensional channels $\mathscr{V}_n^{3d}$ and $\mathscr{S}_n^{3d}$. Data are for: $\mathscr{V}_n^{3d}$: K_{02} (solid line), $-\alpha_{12}$ (broken line); $\mathscr{S}_n^{3d}$: K_{02} (•), $-\alpha_{12}$ (■).

These ordinary integrals are computed with the help of *Mathematica*® with a precision of 15 decimal digits by the standard operator NIntegrate; the number of grid points is not important in computing the integral and it could be increased without any significant time increase. Moreover, all these integrals could be calculated analytically, but it was found more convenient to compute them numerically. As a result, the calculations take about 14 min for the two-dimensional channel $\mathscr{V}_1$ and 62 min for the three-dimensional channel S_n^{3d}. The computations were performed by using a usual notebook with a dual core (2.10 GHz) and a central memory of 2 GB.

It is worth nothing that the Fourier coefficients T_{st} and B_{st} of the walls are arbitrary. Hence, varicose and sinuous channels with longitudinal and transversal oscillations and roughness of the walls can be investigated by a unified approach. Computational restrictions arise when too many non-zero terms T_{st} and B_{st} or terms with too high frequencies ω_{st} ($\omega_{st} > 12$) are taken. The large number of terms T_{st} and B_{st} (more than 14) produce many terms which compose the final solution. For instance, ten terms T_{st} and B_{st} produce auxiliary functions with about thousand terms of different scales (polynomial and exponential functions of $\omega_{st}z$). Though these terms are analytically calculated, introduction of the numerical values of ω_{st} may lead to error accumulation. As a consequence, the relative error may be equal to 6% when terms with a high frequency ω_{st} are present. For the other channels, the numerical error is negligible. Of course, this difficulty can be overcome by increasing the computational precision of *Mathematica*® and by interactive manipulations of the obtained symbolic formulae for Φ_i and $\mathbf{u}$.

7. Conclusion

The previous developments are practically useful for interpreting experiments where roughness is small but cannot be neglected. It should be emphasized that the overall precision is always better than 6%. It provides also quantitative informations on the way a channel should be machined in order to favor a given effect.

Of course, this first work could be extended in several ways. First, further orders in ε can be relatively easily derived and this would allow the study of channels which are much rougher.

Another possibility would be to put different boundary conditions on the solid surfaces such as a constant charge. Then, one could try to use boundary conditions which vary in space such as a zeta potential or a surface charge which would be spatially correlated with the roughness.

Further terms in zeta could possibly be included. However, it is not clear at this stage if significant progress can be made about the non-linear character of the equations.

Appendix A. Solution for the velocity field

A.1. Case $\omega_{st} = 0$

Eq. (58) become

$$\frac{\mathrm{d}^2 u_{nk00}}{\mathrm{d}z^2}(z) = \frac{i\pi}{L} F_{nk00}(z), \quad \frac{\mathrm{d}^2 w_{nk00}}{\mathrm{d}z^2}(z) = \frac{\mathrm{d}g_{nk00}}{\mathrm{d}z}(z) + H_{nk00}(z),$$
$$\frac{\mathrm{d}^2 v_{nk00}}{\mathrm{d}z^2}(z) = \frac{i\pi}{L} G_{nk00}(z), \quad \frac{\mathrm{d}w_{nk00}}{\mathrm{d}z}(z) = 0. \tag{A1}$$

If $n = k = 0$, the Fourier series degenerate and one obtains the classical Poiseuille flow in the plane channel

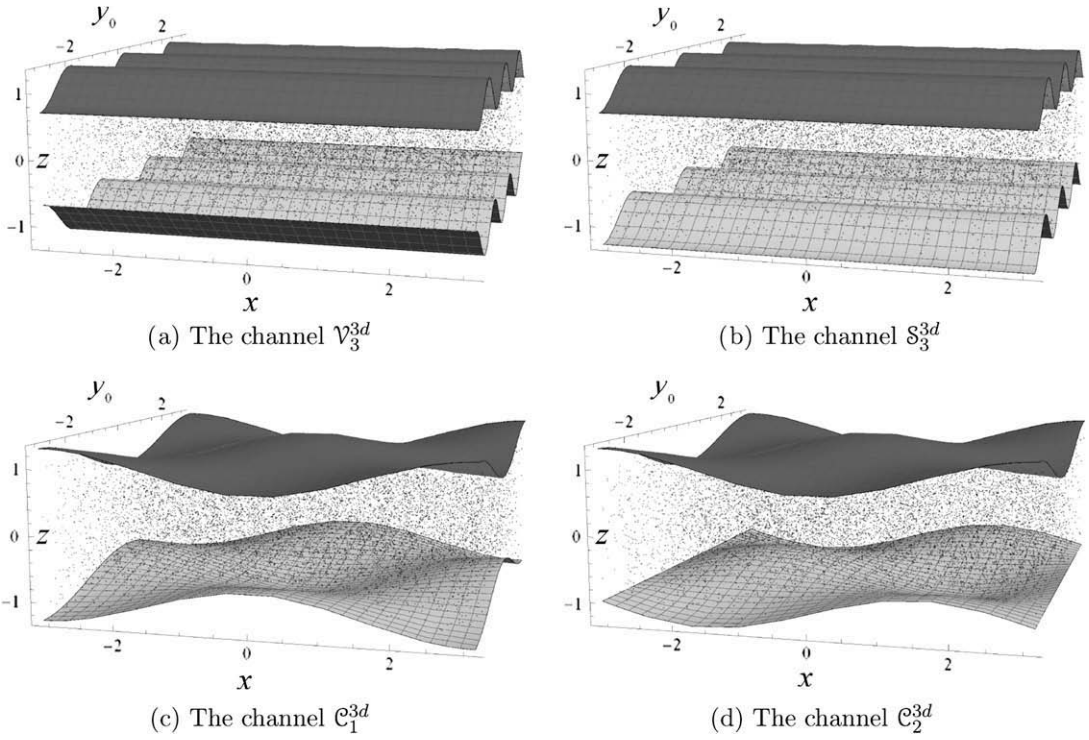

Fig. 8. The three-dimensional channels (see Table 3).

$$u_{00}(x,y,z)=\frac{\overline{\nabla p}}{2}(z^2-b^2),\quad v_{00}(x,y,z)=w_{00}(x,y,z)=0,$$
$$g_{00}(x,y,z)=\overline{\nabla p}x. \tag{A2}$$

If $n\neq 0$ or $k\neq 0$, the general solution of the system (A1) with the boundary conditions (61) has the form

$$\begin{aligned}
u_{nk00}(z)&=C_1+C_2z+\tfrac{i\pi}{L}\textstyle\int_{-b}^{z}(z-\xi)F_{nk00}(\xi)\,\mathrm{d}\xi,\\
v_{nk00}(z)&=D_1+D_2z+\tfrac{i\pi}{L}\textstyle\int_{-b}^{z}(z-\xi)G_{nk00}(\xi)\,\mathrm{d}\xi,\\
w_{nk00}(z)&=\tfrac{1}{2}\left(U_{nk00}^{(3)}+V_{nk00}^{(3)}\right),
\end{aligned} \tag{A3}$$

where the constants C_j and D_j are calculated by

$$\begin{aligned}
C_1&=\tfrac{i\pi}{2L}\left(U_{nk00}^{(1)}+V_{nk00}^{(1)}-\textstyle\int_{-b}^{b}(b-\xi)F_{nk00}(\xi)\,\mathrm{d}\xi\right),\\
C_2&=\tfrac{i\pi}{2bL}\left(U_{nk00}^{(1)}-V_{nk00}^{(1)}-\textstyle\int_{-b}^{b}(b-\xi)F_{nk00}(\xi)\,\mathrm{d}\xi\right),\\
D_1&=\tfrac{i\pi}{2L}\left(U_{nk00}^{(2)}+V_{nk00}^{(2)}-\textstyle\int_{-b}^{b}(b-\xi)G_{nk00}(\xi)\,\mathrm{d}\xi\right),\\
D_2&=\tfrac{i\pi}{2bL}\left(U_{nk00}^{(2)}-V_{nk00}^{(2)}-\textstyle\int_{-b}^{b}(b-\xi)G_{nk00}(\xi)\,\mathrm{d}\xi\right).
\end{aligned} \tag{A4}$$

Here, for instance $U_{nk00}^{(1)}$ denotes the first component of the vector $\mathbf{U}_{nk00}$.

A.2. Case $\omega_{st}\neq 0$

Eqs. (58) are transformed as follows. Differentiate the first and second Eqs. (58) in z. Multiply the results by $\frac{i\pi s}{L}$ and by $\frac{i\pi t}{L}$, respectively. Add the obtained equations with the third equation multiplied by ω_{st}^2. According fourth Eq. (58) replace $\frac{i\pi s}{L}u_{nkst}+\frac{i\pi t}{L}v_{nkst}$ with $-\frac{\mathrm{d}w_{nkst}}{\mathrm{d}z}$. The result is the fourth-order differential equation

$$\frac{\mathrm{d}^4w_{nkst}}{\mathrm{d}z^4}-2\omega_{st}^2\frac{\mathrm{d}^2w_{nkst}}{\mathrm{d}z^2}+\omega_{st}^4w_{nkst}=W_{nkst}, \tag{A5}$$

where W_{nkst} is related to the known functions from the right parts of (58)

$$W_{nkst}(z)=\frac{\pi^2 s}{L^2}\frac{\mathrm{d}F_{nkst}}{\mathrm{d}z}(z)+\frac{\pi^2 t}{L^2}\frac{\mathrm{d}G_{nkst}}{\mathrm{d}z}(z)-\omega_{st}^2H_{nkst}(z). \tag{A6}$$

It follows from (61) that w_{nkst} satisfies the boundary conditions

$$\begin{aligned}
&w_{nkst}(b)=U_{nkst}^{(3)},\quad \frac{\mathrm{d}w_{nkst}}{\mathrm{d}z}(b)=-\frac{i\pi}{L}(sU_{nkst}^{(1)}+tU_{nkst}^{(2)}),\\
&w_{nkst}(-b)=V_{nkst}^{(3)},\quad \frac{\mathrm{d}w_{nkst}}{\mathrm{d}z}(-b)=-\frac{i\pi}{L}(sV_{nkst}^{(1)}+tV_{nkst}^{(2)}).
\end{aligned} \tag{A7}$$

Using long but standard manipulations, the solution of Eqs. (A5) and (A7) is derived as

$$w_{nkst}(z)=(c_1+c_2z)\cosh\omega_{st}z+(d_1+d_2z)\sinh\omega_{st}z+\mathscr{W}_{nkst}(z), \tag{A8}$$

where

$$\begin{aligned}
\mathscr{W}_{nkst}(z)=\frac{1}{2\omega_{st}^3}\Bigg[&\omega_{st}\int_{-b}^{z}(z-\xi)\cosh\omega_{st}\xi W_{nkst}(\xi)\,\mathrm{d}\xi\\
&+\frac{d^2}{dz^2}\left(\int_{-b}^{z}(z-\xi)\cosh\omega_{st}\xi W_{nkst}(\xi)\,\mathrm{d}\xi\right)\Bigg].
\end{aligned} \tag{A9}$$

The constants c_j and d_j are

$$\begin{aligned}
c_1&=\frac{b\omega_{st}(R_1+R_2)\cosh\omega_{st}b+[R_1+R_2-b(R_3-R_4)]\sinh\omega_{st}b}{\sinh 2\omega_{st}b+2\omega_{st}b},\\
c_2&=\frac{b\omega_{st}(R_1-R_2)\sinh\omega_{st}b+[R_1-R_2-b(R_3+R_4)]\cosh\omega_{st}b}{\sinh 2\omega_{st}b-2\omega_{st}b},\\
d_1&=\frac{-\omega_{st}(R_1-R_2)\cosh\omega_{st}b+(R_3-R_4)\sinh\omega_{st}b}{\sinh 2\omega_{st}b-2\omega_{st}b},\\
d_2&=\frac{-\omega_{st}(R_1+R_2)\sinh\omega_{st}b+(R_3-R_4)\cosh\omega_{st}b}{\sinh 2\omega_{st}b+2\omega_{st}b},
\end{aligned} \tag{A10}$$

where

$$\begin{aligned}
&R_1=U_{nkst}^{(3)}-\mathscr{W}_{nkst}(b),\quad R_3=-\frac{i\pi}{L}(sU_{nkst}^{(1)}+tU_{nkst}^{(2)})-\mathscr{W}_{nkst}(b),\\
&R_2=V_{nkst}^{(3)},\quad R_4=-\frac{i\pi}{L}(sV_{nkst}^{(1)}+tV_{nkst}^{(2)}).
\end{aligned} \tag{A11}$$

Formulae (44b), (A8), (A9), (A10) and (A11) completely determine the third component of the velocity, more precisely its Fourier components w_{nkst}.

The first and the second components of the velocity are determined by the following computations. First, generate the linear combination

$$M_{nkst}(z) = tu_{nkst}(z) - sv_{nkst}(z). \tag{A12}$$

Then, the same linear combinations of the first two equations (58) and the boundary conditions (61) yield the ordinary differential equation

$$\frac{\mathrm{d}^2 M_{nkst}}{\mathrm{d}z^2}(z) - \omega_{st}^2 M_{nkst}(z) = N_{nkst}(z) \tag{A13}$$

with the boundary conditions

$$M_{nkst}(b) = tU_{nkst}^{(1)} - sU_{nkst}^{(2)}, \qquad M_{nkst}(-b) = tV_{nkst}^{(1)} - sV_{nkst}^{(2)}. \tag{A14}$$

The functions N_{nkst} are defined by

$$N_{nkst}(z) = \frac{i\pi}{L}\left[tF_{nkst}(z) - sG_{nkst}(z)\right] \tag{A15}$$

The solution of the boundary value problem (A13) and (A14) is

$$M_{nkst}(z) = [C_1 - c(z)]\cosh\omega_{st}z + [C_2 + s(z)]\sinh\omega_{st}z, \tag{A16}$$

where the functions $c(z)$ and $s(z)$ are

$$c(z) = \frac{1}{\omega_{st}}\int_{-b}^{z} N_{nkst}(\xi)\cosh\omega_{st}\xi\,\mathrm{d}\xi,$$
$$s(z) = \frac{1}{\omega_{st}}\int_{-b}^{z} N_{nkst}(\xi)\sinh\omega_{st}\xi\,\mathrm{d}\xi. \tag{A17}$$

The constants C_j are given by

$$C_1 = \frac{t(U_{nkst}^{(1)} - V_{nkst}^{(1)}) - s(U_{nkst}^{(2)} - V_{nkst}^{(2)}) + c(b) - s(b)}{2\omega_{st}\sinh\omega_{st}b}, \tag{A18}$$
$$C_2 = \frac{t(U_{nkst}^{(1)} - V_{nkst}^{(1)}) + s(U_{nkst}^{(2)} + V_{nkst}^{(2)}) + c(b) - s(b)}{2\omega_{st}\cosh\omega_{st}b}.$$

Therefore, the function $M_{nkst}(z)$ is determined by Eqs. (A16)–(A18).

The functions $u_{nkst}(z)$ and $v_{nkst}(z)$ are found from the following relations

$$tu_{nkst}(z) - sv_{nkst}(z) = M_{nkst}(z), \qquad su_{nkst}(z) + tv_{nkst}(z) = \frac{iL}{\pi}\frac{\mathrm{d}w_{nkst}}{\mathrm{d}z}(z). \tag{A19}$$

Hence,

$$u_{nkst}(z) = \frac{i\pi s}{L\omega_{st}^2}\frac{\mathrm{d}w_{nkst}}{\mathrm{d}z}(z) + \frac{\pi^2 t}{L^2\omega_{st}^2}M_{nkst}(z),$$
$$v_{nkst}(z) = \frac{i\pi t}{L\omega_{st}^2}\frac{\mathrm{d}w_{nkst}}{\mathrm{d}z}(z) - \frac{\pi^2 s}{L^2\omega_{st}^2}M_{nkst}(z). \tag{A20}$$

The functions $M_{nkst}(z)$ and $w_{nkst}(z)$ are given by (A16) and (A8).

Appendix B. The coupling coefficient

B.1. Determination of $\langle\psi u\rangle$

Let us study the integral in z in the triple integral (64). Let $f(x,y,z)$ denote a smooth function and $F(x,y,z)$ its primitive in z, i.e., $\frac{\partial}{\partial z}F(x,y,z) = f(x,y,z)$. Introduce

$$\mathscr{F}(x,y) = \int_{-b+b\varepsilon B(x,y)}^{b+b\varepsilon T(x,y)} f(x,y,z)\,\mathrm{d}z = F(x,y,b+b\varepsilon T(x,y)) - F(x,y,-b+b\varepsilon B(x,y)). \tag{B1}$$

Application of the Taylor formula (29) yields

$$\mathscr{F}(x,y) = \sum_{k=0}^{\infty}\frac{b^k\varepsilon^k}{k!}\left[T^k\frac{\partial^k F}{\partial z^k}(x,y,b) - B^k\frac{\partial^k F}{\partial z^k}(x,y,-b)\right]. \tag{B2}$$

Hence, the integral (B1) with variable limits of integration is reduced to

$$\mathscr{F}(x,y) = \int_{-b}^{b} f(x,y,z)\,\mathrm{d}z + \sum_{k=1}^{\infty} \times \frac{b^k\varepsilon^k}{k!}\left[T^k\frac{\partial^{k-1} f}{\partial z^{k-1}}(x,y,b) - B^k\frac{\partial^{k-1} f}{\partial z^{k-1}}(x,y,-b)\right]. \tag{B3}$$

Substitute $f = \psi u$ into (B3) and preserve the terms of order $O(\varepsilon^2)$

$$\begin{aligned}\mathscr{A}(x,y) = \int_{-b+b\varepsilon B(x,y)}^{b+b\varepsilon T(x,y)}\psi u\,\mathrm{d}z = \int_{-b}^{b}\psi u\,\mathrm{d}z + \varepsilon b[&T(x,y)\psi(x,y,b)u(x,y,b) \\ &- B(x,y)\psi(x,y,-b)u(x,y,-b)] + \frac{b^2\varepsilon^2}{2}\Big[T^2(x,y)\Big(u(x,y,b)\frac{\partial\psi}{\partial z}(x,y,b) \\ &+\psi(x,y,b)\frac{\partial u}{\partial z}(x,y,b)\Big) - B^2(x,y)\Big(u(x,y,-b)\frac{\partial\psi}{\partial z}(x,y,-b) \\ &+\psi(x,y,-b)\frac{\partial u}{\partial z}(x,y,-b)\Big)\Big] + O(\varepsilon^3).\end{aligned} \tag{B4}$$

The functions ψ and u are calculated in Section 3 and in Section 4.2 in the form of expansion in ζ, ε and the Fourier series in x, y. Hence, it is convenient to present (B4) in such a form. First, expansions in ζ and ε are applied. Then, $\mathscr{A}(x,y)$ defined by (B4) becomes

$$\mathscr{A}(x,y) = \sum_{n,k=0}^{\infty}\zeta^n\varepsilon^k a_{nk}(x,y), \tag{B5}$$

where the required terms with $k = 0, 1, 2$ can be written as

$$a_{n0}(x,y) = \int_{-b}^{b}\cosh z\; u_{n-1,0}(x,y,z)\,\mathrm{d}z, \tag{B6}$$

$$a_{n1}(x,y) = \int_{-b}^{b}(\psi_1 u_{n-1,0} + \cosh z\; u_{n-1,1})\,\mathrm{d}z + b \times \cosh b\left[T\psi_0 u_{n-1,0}|_{z=b} - B\psi_0 u_{n-1,0}|_{z=-b})\right],$$

$$\begin{aligned}a_{n2}(x,y) = \int_{-b}^{b}(\psi_2 u_{n-1,0} + \psi_1 u_{n-1,1} + \cosh z\; u_{n-1,2})\,\mathrm{d}z + b[&T(\psi_1 u_{n-1,0} \\ &+ \cosh b\; u_{n-1,1})|_{z=b} - B(\psi_1 u_{n-1,0} + \cosh b\; u_{n-1,1})|_{z=-b}] \\ &+ \frac{b^2\sinh b}{2}(T^2 u_{n-1,0}|_{z=b} + B^2 u_{n-1,0}|_{z=-b}) \\ &+ \frac{b^2\cosh b}{2}\left(T^2\frac{\partial u_{n-1,0}}{\partial z}|_{z=b} - B^2\frac{\partial u_{n-1,0}}{\partial z}|_{z=-b}\right).\end{aligned}$$

where the arguments of the functions are omitted for shortness.

The next step is the calculation of the integrals in x and y in (64)

$$\langle\psi u\rangle = \frac{1}{8bL^2}\int_{-L}^{L}\int_{-L}^{L}\mathscr{A}(x,y)\,\mathrm{d}x\,\mathrm{d}y = \frac{1}{2b}\sum_{n,k=0}^{\infty}\zeta^n\varepsilon^k A_{nk}, \tag{B7}$$

where

$$A_{nk} = \int_{-L}^{L}\int_{-L}^{L} a_{nk}(x,y)\,\mathrm{d}x\,\mathrm{d}y. \tag{B8}$$

The functions ψ_1 and ψ_2 were calculated in Section 3 as Fourier series as well as the functions $u_{n-1,0}$ and $u_{n-1,1}$ in Section 4.2 with the computed coefficients $u_{n-1,0st}$. Substitution of these formulae into (B6) and into (B7) yields after some tedious symbolic computations

$$A_{0k} = 0, \quad A_{n0} = \int_{-b}^{b}\cosh z\; u_{n-1,0}\,\mathrm{d}z, \tag{B9}$$

Table C.1
The coefficients K_{nk} for the two-dimensional varicose channels described in Table 1.

Channel	K_{00}	K_{02}	K_{22}	K_{32}	K_{42}
$\mathscr{V}_1$	0.05305165	−0.19064676	−0.00022889	−0.00000255	0.00000033
$\mathscr{V}_2$	0.05305165	−0.27998459	−0.00005912	−0.00000044	0.00000005
$\mathscr{V}_3$	0.05305165	−0.41009148	−0.00001309	−0.00000006	0.00000001
$\mathscr{V}_4$	0.05305165	−0.56004845	−0.00000325	−0.00000001	−0.00000000
$\mathscr{V}_5$	0.05305165	−0.71684814	−0.00000102	−0.00000000	0.00000002
$\mathscr{V}_6$	0.05305165	−0.87548129	−0.00000041	−0.00000419	0.00000594
$\mathscr{V}_7$	0.05305165	−1.03453122	−0.00000020	0.00000542	0.00000496
$\mathscr{V}_8$	0.05305165	−1.19366637	0.00008958	0.00006989	0.00004525
$\mathscr{V}_9$	0.05305165	−1.35281776	0.00008128	0.00006799	−0.00199125
$\mathscr{V}_{10}$	0.05305165	−1.51197208	0.00083152	−0.00274530	−0.00034320
$\mathscr{V}_{11}$	0.05305165	−1.67112692	−0.03283528	−0.00021212	0.00478510
$\mathscr{V}_{12}$	0.05305165	−1.83028185	−0.03618856	−0.00040601	0.00539587

Table C.2
The coefficients K_{nk} for the two-dimensional sinuous channels given in Table 1.

Channel	K_{00}	K_{02}	K_{22}	K_{32}	K_{42}
$\mathscr{S}_1$	0.05305165	−0.05512055	−0.00000001	0.00000000	0.00056619
$\mathscr{S}_2$	0.05305165	−0.20839997	−0.00000062	0.00000000	0.00000000
$\mathscr{S}_3$	0.05305165	−0.38639969	−0.00000145	−0.00000000	0.00000000
$\mathscr{S}_4$	0.05305165	−0.55406854	−0.00000118	−0.00000000	−0.00000000
$\mathscr{S}_5$	0.05305165	−0.71554753	−0.00000068	−0.00000000	0.00000002
$\mathscr{S}_6$	0.05305165	−0.87522313	−0.00000036	−0.00000418	0.00000594
$\mathscr{S}_7$	0.05305165	−1.03448304	−0.00000019	0.00000542	0.00000496
$\mathscr{S}_8$	0.05305165	−1.19365777	0.00008958	0.00006989	0.00004525
$\mathscr{S}_9$	0.05305165	−1.35281627	0.00008126	0.00006800	−0.00199125
$\mathscr{S}_{10}$	0.05305165	−1.51197183	0.00083141	−0.00274529	−0.00034327
$\mathscr{S}_{11}$	0.05305165	−1.67112688	−0.03283578	−0.00021208	0.00478490
$\mathscr{S}_{12}$	0.05305165	−1.83028184	−0.03617176	−0.00040677	0.00540160

Table C.3
The coefficients K_{nk} for the two-dimensional channels $\mathscr{I}_{nk}$ given in Table 1.

Channel	K_{00}	K_{02}	K_{22}	K_{32}	K_{42}
$\mathscr{I}_3$	0.05305165	−0.16024447	−0.00013287	−0.00000144	0.00000018
$\mathscr{I}_4$	0.05305165	−0.16174404	−0.00013277	−0.00000135	0.00000025
$\mathscr{I}_5$	0.05305165	−0.16331203	−0.00013275	−0.00000138	0.00000062
$\mathscr{I}_6$	0.05305165	−0.16489836	−0.00013162	−0.00000078	0.00000054
$\mathscr{I}_7$	0.05305165	−0.16648886	−0.00012453	−0.00001584	−0.00001379
$\mathscr{I}_8$	0.05305165	−0.16808022	−0.00012447	−0.00002143	0.00003513
$\mathscr{I}_9$	0.05305165	−0.16967173	−0.00039421	0.00000071	0.00003885
$\mathscr{I}_{10}$	0.05305165	−0.17126327	−0.00042075	−0.00000479	−0.00002328
$\mathscr{I}_{11}$	0.05305165	−0.17285482	−0.00012420	−0.00003932	0.00001347
$\mathscr{I}_{12}$	0.05305165	−0.17444637	−0.00049676	−0.00000823	−0.00001015

Table C.4
The coefficients α_{nk} for the two-dimensional varicose channels given in Table 1.

Channel	α_{10}	α_{12}	α_{32}	α_{42}	α_{52}
$\mathscr{V}_1$	−0.03794347	0.09129521	0.00016049	0.00000179	−0.00000023
$\mathscr{V}_2$	−0.03794347	0.14677744	0.00004118	0.00000030	−0.00000004
$\mathscr{V}_3$	−0.03794347	0.23146311	0.00000902	0.00000004	−0.00000001
$\mathscr{V}_4$	−0.03794347	0.33086870	0.00000220	0.00000001	0.00000000
$\mathscr{V}_5$	−0.03794347	0.43549855	0.00000068	−0.00000048	0.00000019
$\mathscr{V}_6$	−0.03794347	0.54160677	0.00000027	0.00000583	−0.00000385
$\mathscr{V}_7$	−0.03794347	0.64810002	0.00000008	−0.00000491	0.00000836
$\mathscr{V}_8$	−0.03794347	0.75470479	−0.00003004	−0.00003684	−0.00003527
$\mathscr{V}_9$	−0.03794347	0.86135372	0.00007143	−0.00022910	0.00125493
$\mathscr{V}_{10}$	−0.03794347	0.96802724	0.00005155	0.00119961	0.00050676
$\mathscr{V}_{11}$	−0.03794347	1.07471737	0.02502505	0.00058048	0.00032893
$\mathscr{V}_{12}$	−0.03794347	1.18015709	−0.00018679	0.00072894	−0.00018404

Table C.5
The coefficients α_{nk} for the two-dimensional sinuous channels given in Table 1.

Channel	α_{10}	α_{12}	α_{32}	α_{42}	α_{52}
$\mathscr{S}_1$	−0.03794347	−0.00513099	0.00000001	−0.00000000	−0.00043930
$\mathscr{S}_2$	−0.03794347	0.09531903	0.00000038	−0.00000000	−0.00000000
$\mathscr{S}_3$	−0.03794347	0.21423798	0.00000093	0.00000000	−0.00000000
$\mathscr{S}_4$	−0.03794347	0.32648395	0.00000077	0.00000000	0.00000000
$\mathscr{S}_5$	−0.03794347	0.43453907	0.00000044	−0.00000048	0.00000019
$\mathscr{S}_6$	−0.03794347	0.54141547	0.00000023	0.00000583	−0.00000385
$\mathscr{S}_7$	−0.03794347	0.64806420	0.00000007	−0.00000491	0.00000836
$\mathscr{S}_8$	−0.03794347	0.75469838	−0.00003004	−0.00003684	−0.00003527
$\mathscr{S}_9$	−0.03794347	0.86135262	0.00007144	−0.00022910	0.00125493
$\mathscr{S}_{10}$	−0.03794347	0.96802705	0.00005163	0.00119960	0.00050681
$\mathscr{S}_{11}$	−0.03794347	1.07471734	0.02502542	0.00058045	0.00032908
$\mathscr{S}_{12}$	−0.03794347	1.18015709	−0.00019959	0.00072953	−0.00018840

Table C.6
The coefficients α_{nk} for the two-dimensional channels $\mathscr{I}_{nk}$ given in Table 1.

Channel	α_{10}	α_{12}	α_{32}	α_{42}	α_{52}
$\mathscr{I}_3$	−0.03794347	0.07959608	0.00009311	0.00000100	−0.00000013
$\mathscr{I}_4$	−0.03794347	0.08059014	0.00009305	0.00000097	−0.00000013
$\mathscr{I}_5$	−0.03794347	0.08163643	0.00009276	0.00000117	−0.00000040
$\mathscr{I}_6$	−0.03794347	0.08269752	0.00009292	0.00000067	−0.00000161
$\mathscr{I}_7$	−0.03794347	0.08376245	0.00009493	0.00000783	0.00000860
$\mathscr{I}_8$	−0.03794347	0.08482850	0.00009372	0.00002038	−0.00001446
$\mathscr{I}_9$	−0.03794347	0.08589499	0.00009170	0.00000249	0.00000193
$\mathscr{I}_{10}$	−0.03794347	0.08694657	0.00011609	0.00000703	0.00005240
$\mathscr{I}_{11}$	−0.03794347	0.08801485	0.00008652	−0.00145663	−0.00001025
$\mathscr{I}_{12}$	−0.03794347	0.08908302	0.00037026	−0.00177141	0.00000774

Table C.7
The coefficients A_{nk} for the two-dimensional varicose channels given in Table 1.

Channel	A_{00}	A_{02}	A_{22}	A_{32}	A_{42}
$\mathscr{V}_1$	−0.71521753	−0.84933637	−0.00006052	−0.00000069	0.00000009
$\mathscr{V}_2$	−0.71521753	−1.00793189	−0.00002069	−0.00000017	0.00000002
$\mathscr{V}_3$	−0.71521753	−1.16568504	−0.00000653	−0.00000004	−0.00000004
$\mathscr{V}_4$	−0.71521753	−1.31358346	−0.00000231	−0.00000001	−0.00000001
$\mathscr{V}_5$	−0.71521753	−1.45525755	−0.00000097	−0.00000915	0.00000383
$\mathscr{V}_6$	−0.71521753	−1.59378261	−0.00000047	0.00005348	0.00000746
$\mathscr{V}_7$	−0.71521753	−1.73066907	−0.00000122	−0.00001941	0.00022447
$\mathscr{V}_8$	−0.71521753	−1.86660236	0.00064139	0.00024783	−0.00005486
$\mathscr{V}_9$	−0.71521753	−2.00192187	0.00244210	−0.00340180	−0.00319022
$\mathscr{V}_{10}$	−0.71521753	−2.13681776	0.01218180	−0.01439876	0.00492528
$\mathscr{V}_{11}$	−0.71521753	−2.27140742	0.02904112	0.00808209	0.07071056
$\mathscr{V}_{12}$	−0.71521753	−2.42956783	−0.49139824	0.00826654	0.06927557

Table C.8
The coefficients A_{nk} for the two-dimensional sinuous channels given in Table 1.

Channel	A_{00}	A_{02}	A_{22}	A_{32}	A_{42}
$\mathscr{S}_1$	−0.71521753	−0.83982648	−0.00000006	0.00000000	−0.00064751
$\mathscr{S}_2$	−0.71521753	−1.01282960	−0.00000126	0.00000000	0.00000000
$\mathscr{S}_3$	−0.71521753	−1.17096935	−0.00000202	−0.00000000	−0.00000004
$\mathscr{S}_4$	−0.71521753	−1.31561574	−0.00000144	−0.00000000	−0.00000001
$\mathscr{S}_5$	−0.71521753	−1.45580910	−0.00000082	−0.00000913	0.00000382
$\mathscr{S}_6$	−0.71521753	−1.59390815	−0.00000044	0.00005347	0.00000746
$\mathscr{S}_7$	−0.71521753	−1.73069478	−0.00000121	−0.00001941	0.00022447
$\mathscr{S}_8$	−0.71521753	−1.86660727	0.00064139	0.00024783	−0.00005486
$\mathscr{S}_9$	−0.71521753	−2.00192276	0.00244212	−0.00340180	−0.00319022
$\mathscr{S}_{10}$	−0.71521753	−2.13681792	0.01218189	−0.01439877	0.00492534
$\mathscr{S}_{11}$	−0.71521753	−2.27140744	0.02904155	0.00808205	0.07071076
$\mathscr{S}_{12}$	−0.71521753	−2.42956784	−0.49141293	0.00826742	0.06927054

Table C.9
The coefficients A_{nk} for the two-dimensional channels $\mathscr{I}_{nk}$ given in Table 1.

Channel	A_{00}	A_{02}	A_{22}	A_{32}	A_{42}
$\mathscr{I}_3$	−0.71521753	−0.65999027	−0.00003617	−0.00000052	0.00000010
$\mathscr{I}_4$	−0.71521753	−0.66146926	−0.00003612	0.00000008	0.00000092
$\mathscr{I}_5$	−0.71521753	−0.66288600	−0.00004121	0.00000350	0.00000079
$\mathscr{I}_6$	−0.71521753	−0.66427125	−0.00002291	0.00000214	−0.00002310
$\mathscr{I}_7$	−0.71521753	−0.66564011	0.00011057	−0.00006591	−0.00002378
$\mathscr{I}_8$	−0.71521753	−0.66699945	0.00008848	0.00009517	0.00020095
$\mathscr{I}_9$	−0.71521753	−0.66835264	−0.00358602	0.00005649	0.00056008
$\mathscr{I}_{10}$	−0.71521753	−0.66998720	−0.00348405	0.00006803	0.00067395
$\mathscr{I}_{11}$	−0.71521753	−0.67130713	−0.00004356	−0.02798686	−0.00001157
$\mathscr{I}_{12}$	−0.71521753	−0.67262910	0.00028212	−0.03350128	0.00000908

Table C.10
The coefficients $K = 0.05305165 + K_{02}\varepsilon^2$, $\alpha = -0.03794347\zeta + \alpha_{12}\zeta\varepsilon^2$ and $A = -0.71521753 + A_{02}\varepsilon^2$ for the three-dimensional varicose $\mathscr{V}_n^{3d}$ and sinuous $\mathscr{S}_n^{3d}$ channels given in Table 3.

n	Channel $\mathscr{V}_n^{3d}$			Channel $\mathscr{S}_n^{3d}$		
	K_{02}	α_{12}	A_{02}	K_{02}	α_{12}	A_{02}
1	0.07957747	−0.11854742	−1.16173991	0.07957747	−0.12339534	−1.25312100
2	0.07957747	−0.13197311	−1.41480826	0.07957747	−0.13344953	−1.44263802
3	0.07957747	−0.14592203	−1.67773913	0.07957747	−0.14624950	−1.68391181
4	0.07957747	−0.15993701	−1.94191525	0.07957747	−0.15999950	−1.94309321
5	0.07957747	−0.17406350	−2.20819347	0.07957747	−0.17407448	−2.20840035
6	0.07957747	−0.18828195	−2.47620476	0.07957747	−0.18828378	−2.47623927
7	0.07957747	−0.20256250	−2.74538690	0.07957747	−0.20256280	−2.74539245
8	0.07957747	−0.21688409	−3.01534254	0.07957747	−0.21688414	−3.01534341
9	0.07957747	−0.23123357	−3.28582388	0.07957747	−0.23123358	−3.28582401
10	0.07957747	−0.24560273	−3.55667615	0.07957747	−0.24560273	−3.55667617
11	0.07957747	−0.25998626	−3.82779934	0.07957747	−0.25998627	−3.82779934
12	0.07957747	−0.27438061	−4.09912629	0.07957747	−0.27438061	−4.09912629

$$A_{n1} = \int_{-b}^{b} \cosh z\; u_{n-1,100}\,\mathrm{d}z + \sum_{st}\int_{-b}^{b} \psi_{1,-s,-t}\; u_{n-1,0st}\,\mathrm{d}z + b \times \cosh b \sum_{st}(T_{-s,-t}U^{(1)}_{n-1,0st} - B_{-s,-t}V^{(1)}_{n-1,0st}),$$

$$\begin{aligned} A_{n2} = {} & \int_{-b}^{b} \cosh z\; u_{n-1,200}\,\mathrm{d}z + \sum_{st}\int_{-b}^{b}(\psi_{2,-s,-t}\; u_{n-1,0st} \\ & + \psi_{1,-s,-t}\; u_{n-1,1st})\,\mathrm{d}z + b\cosh b \sum_{st}(T_{-s,-t}U^{(1)}_{n-1,1st} \\ & - B_{-s,-t}V^{(1)}_{n-1,1st}) - b^2\tanh b\sum_{st}\sum_{pq}(T_{-s-p,-t-q}T_{st}U^{(1)}_{n-1,0pq} \\ & + B_{-s-p,-t-q}B_{st}V^{(1)}_{n-1,0pq}) + \frac{b^2\sinh b}{2}\sum_{st}\sum_{pq}(T_{-s-p,-t-q}T_{pq}U^{(1)}_{n-1,0st} \\ & - B_{-s-p,-t-q}B_{pq}V^{(1)}_{n-1,0st}) + \frac{b^2\cosh b}{2}\sum_{st} \\ & \times \sum_{pq}\left(T_{-s-p,-t-q}T_{pq}\frac{\mathrm{d}u_{n-1,0st}}{\mathrm{d}z}(b) - B_{-s-p,-t-q}B_{pq}\frac{\mathrm{d}u_{n-1,0st}}{\mathrm{d}z}(-b)\right). \end{aligned}$$

Therefore, the expression $\langle\psi u\rangle$ can be computed by (B7) and (B9) with an accuracy $O(\varepsilon^2)$ and $O(\zeta^4)$.

B.2. Determination of $\langle u\rangle$

Similar computations can be applied to $\langle u\rangle$. It was already done in [15] for Stokes flow only without any electrical effect with an accuracy $O(\varepsilon^{30})$. Below the results are given for $\langle u\rangle$ when the electric potential is taken into account, but without an external electric field. Numerical comparison shows a weak dependence on ζ (see examples below). $\langle u\rangle$ is given by

$$\langle u\rangle = \frac{1}{2b}\sum_{n,k=0}^{\infty}\zeta^n\varepsilon^k K_{nk}, \tag{B10}$$

where

$$\begin{aligned} K_{n0} = {} & \int_{-b}^{b} u_{n000}\,\mathrm{d}z, \quad K_{n1} \\ = {} & \int_{-b}^{b} u_{n100}\,\mathrm{d}z + b\sum_{st}(T_{-s,-t}U^{(1)}_{n,0st} - B_{-s,-t}V^{(1)}_{n,0st}), \end{aligned} \tag{B11}$$

$$\begin{aligned} K_{n2} = {} & \int_{-b}^{b} u_{n200}\,\mathrm{d}z + b\sum_{st}(T_{-s,-t}U^{(1)}_{n,1st} - B_{-s,-t}V^{(1)}_{n,1st}) + \frac{b^2}{2}\sum_{st} \\ & \times \sum_{pq}\left(T_{-s-p,-t-q}T_{pq}\frac{\mathrm{d}u_{n,0st}}{\mathrm{d}z}((b) - B_{-s-p,-t-q}B_{pq}\frac{\mathrm{d}u_{n,0st}}{\mathrm{d}z}(-b)\right). \end{aligned}$$

Appendix C. Complete numerical data

C.1. Two-dimensional channels

See Tables C.1–C.9.

C.2. Three-dimensional channels

Table C.10.

References

[1] G.E. Karniadakis, A. Beskok, N. Aluru, Microflows and Nanoflows: Fundamentals and Simulation, Springer, New York, 2005.
[2] D. Coelho, M. Shapiro, J.E. Thovert, P.M. Adler, J. Colloid Interface Sci. 181 (1996) 169.
[3] P.M. Adler, Math. Geol. 33 (2001) 63.
[4] J.L. Auriault, T. Strzelecki, Int. J. Eng. Sci. 19 (1981) 915.

[5] C. Moyne, M.A. Murad, Transp. Porous Media 62 (2006) 333.
[6] C. Moyne, M.A. Murad, Transp. Porous Media 63 (2006) 13.
[7] J.R. Looker, S.L. Carnie, Transp. Porous Media 65 (2006) 131.
[8] R. Qiao, N.R. Aluru, Phys. Rev. Lett. 92 (2004) 198301.
[9] Shizhi Qian, Haim H. Bau, Appl. Math. Modell. 29 (2005) 726.
[10] E. Brunet, A. Ajdari, Phys. Rev. E 73 (2006) 056306.
[11] N.A. Patankar, H.H. Hu, Anal. Chem. 70 (1998) 1870.
[12] Y.Q. Zu, Y.Y. Yan, J. Bionic Eng. 3 (2006) 179.
[13] Y. Gao, T.N. Wong, C. Yang, N.T. Nguyen, K.T. Ooi, C. Wang, J. Phys.: Conf. Ser. 34 (2006) 470.
[14] A. Gupta, D. Coelho, P.M. Adler, J. Colloid Interface Sci. 319 (2008) 549.
[15] A.E. Malevich, V.V. Mityushev, P.M. Adler, Acta Mech. 182 (2006) 151.
[16] H.S. Carslaw, J.C. Jaeger, Conduction of Heat in Solids, Clarendon Press, Oxford, 1996.
[17] J. Happel, H. Brenner, Low Reynolds Number Hydrodynamics, Prentice Hall, 1965.
[18] M. Rosanne, M. Paszkuta, P.M. Adler, J. Colloid Interface Sci. 297 (2006) 353.